# A chromosome-level genome reveals the 3D architecture of odorant receptors and their role in the social behaviors of a parasitoid wasp

Zi Ye[1, 2, †], Stephen T. Ferguson[2, †], Guanzhen Fan[2, 3, †], Juan F. Ortiz[4], Zhijie Yan[1], Tao Guan[1], Xingyue Zhang[1], Feng Liu[2, 5, *]

1. School of Life Sciences, Guizhou Normal University, Guiyang, China

2. Institute of Infectious Diseases, Shenzhen Bay Laboratory, Shenzhen, China

3. School of Pharmaceutical Science and Technology, Faculty of Medicine, Tianjin University, Tianjin, China.

4. Paratus Sciences, Singapore, Singapore

5. Guangdong Provincial Key Laboratory of Infection Immunity and Inflammation, Shenzhen, China

[†]Equal contribution

*Correspondence: liufeng@szbl.ac.cn

## Abstract

The emergence of social behaviors in insects is closely linked to the evolution of olfactory systems, yet the genomic mechanisms that shape chemoreceptor expansion and their behavioral outputs remain poorly understood. The subsocial ectoparasitoid wasp *Sclerodermus guani* (Hymenoptera: Bethylidae), a widely employed biocontrol agent against wood-boring pests, relies on olfaction to coordinate host-seeking, reproduction, and cooperative maternal care, providing a tractable system to investigate these relationships in a transitional subsocial species.

Here, we present a chromosome-level genome assembly for *S. guani* and integrate chromatin conformation, transcriptomics, electrophysiology, and functional genetics to examine the organization and behavioral significance of odorant receptor (OR) expansion. We identify 182 chemosensory receptors, including 148 ORs marked by tandem expansion and sex-biased antennal expression. These OR loci preferentially occupy interaction-rich topologically associating domain (TAD) interiors characterized by elevated interaction frequency and reduced boundary insulation. While tandem arrays genome-wide are enriched in such permissive chromatin environments, OR singletons unexpectedly share similar positional bias, suggesting that OR loci are intrinsically embedded within chromatin neighborhoods poised for duplication and coordinated regulation.

To test the functional consequences of this expanded and structurally organized receptor family, we generated a heritable null mutation in the conserved OR co-receptor (*Orco*). *Orco* mutants displayed severe impairments in host localization, mating efficiency, and most strikingly, a collapse of oviposition fidelity and maternal care. Notably, mutants frequently laid eggs indiscriminately, including on conspecific larvae, indicating a loss of kin recognition and raising the possibility that OR-mediated olfaction contributes to the evolutionary transition from solitary parasitism to maternal care in this lineage.

Together, these findings suggest that three-dimensional genome organization may bias the diversification and regulation of chemosensory gene families, and that OR-mediated olfaction is necessary for coordinated reproduction, discriminative parasitism, and maternal care in a subsocial insect.

**Keywords:** *Sclerodermus guani*, genome assembly, odorant receptor, Orco, CRISPR/Cas9, genome architecture, maternal care, parasitism

## Introduction

*Sclerodermus guani* (Hymenoptera: Bethylidae) is an ectoparasitoid wasp indigenous to China that has been widely employed as a biocontrol agent against various wood-boring beetles, most notably *Monochamus alternatus* (Coleoptera: Cerambycidae), the primary vector of pine wilt disease [1]. This species exhibits a complex life history that integrates parasitism with subsocial maternal care [2–4]. The parasitic cycle begins when a female wasp injects venom into a larval host. After injecting her paralytic venom, the female oviposits eggs along the cuticle. Unlike most solitary parasitoid wasps, *S. guani* exhibits a marked degree of sociality that includes specialized, and in some cases, cooperate maternal care behaviors. In several *Sclerodermus* species, females monitor, reposition, and aggregate larval offspring to facilitate collective cocoon spinning [3,5–8]. Curiously, females provide care indiscriminately to both their own and foreign offspring [5], effectively allowing them to serve as collaborative "stepmothers." This combination of host exploitation and parental coordination places *S. guani* in a transitional social context, distinct from both strictly solitary parasitoids and eusocial Hymenoptera.

Olfaction plays a critical role throughout the parasitic lifecycle of *S. guani*, particularly for host detection and kin recognition by females. Previous studies have shown that females detect chemical cues emitted by disease-transmitting pine sawyer beetles, enabling them to discriminate between suitable hosts and non-host substrates [9–12]. In contrast, the male olfactory system is likely specialized for mating, detecting female-emitted volatiles to locate potential mates within cocoons [13]. Because these behaviors are heavily dependent on chemical recognition—including host-emitted volatiles and intraspecific cues—*S. guani* represents an ideal system to investigate how olfactory signaling supports both ecological and social functions.

In wasps and other insects, the antenna plays a central role in sensory perception, housing sensilla that contain neurons responsible for olfaction, gustation, mechanoreception, and hygro-/thermosensation [14,15]. Chemosensory perception among these neurons is mediated by three major receptor families: odorant receptors (ORs), gustatory receptors (GRs), and ionotropic receptors (IRs) [16–18]. GRs primarily detect nonvolatile compounds such as sugars, bitter substances, and carbon dioxide [19–23]. Notably, however, the canonical $CO_2$-detecting GRs found in Diptera appear to be absent from most Hymenoptera, suggesting that $CO_2$ perception in this lineage may occur through alternative chemosensory mechanisms [24]. IRs represent a divergent class of ionotropic glutamate receptors that function in the detection of acids, amines, humidity, and temperature cues [18,25,26]. In contrast, ORs are specialized for the detection of volatile odorants and constitute the principal receptor class mediating long-range olfactory behaviors in insects [27,28].

Insect ORs function as ligand-gated ion channels composed of a divergent, ligand-binding tuning OR subunit and a conserved odorant receptor co-receptor (Orco), typically

assembled in a 1:3 heteromeric complex [29,30]. Volatile ligands bind to specific tuning ORs, presumably facilitated by odorant-binding proteins (OBPs), thereby activating neuronal signals that are subsequently processed in higher olfactory centers [31,32]. Across Hymenoptera, OR gene families have undergone extensive lineage-specific expansions, frequently organized in tandem arrays generated through repeated local duplication events [33–37]. Such expansions, most notably members of the Hymenoptera-specific 9-exon subclade, have been proposed to encode receptors for detecting ecologically and socially relevant chemical cues, consistent with studies in ants demonstrating that OR signaling is necessary for nestmate recognition and other social behaviors [33,38–43]. Interestingly, tandem organization of OR clusters may also influence their regulatory architecture, with recent studies demonstrating that transcriptional interference within OR arrays contributes to monogenic receptor expression [44]. Moreover, emerging evidence suggests that three-dimensional (3D) genome organization can influence gene regulation and structural variation [45–47]. Whether ORs are embedded within such higher-order genomic contexts has not been systematically examined. Together, these findings raise the possibility that genomic organization and chromatin context may play an important role in shaping the evolutionary expansion and coordinated regulation of OR repertoires.

While individual ORs determine ligand specificity, Orco is essential for receptor complex assembly, trafficking, membrane localization, transcriptional regulation, and signal transduction [28,48–50]. Disruption of Orco function therefore provides a powerful genetic approach for interrogating the behavioral roles of OR-mediated olfaction. Studies in Hymenopterans, however, have been relatively limited by the difficulty of generating heritable germline mutations in eusocial species [51]. Nevertheless, genetic disruption of *Orco* in ants was shown to cause profound defects in neural development and social behavior [41,42], while somatic knockout in honey bees revealed both neuronal and transcriptomic deficits [52]. In parasitoid wasps, *Orco* knockdown impaired host-seeking and mating behaviors [53]. Despite these advances, stable germline knockouts remain a persistent challenge due to the unique reproductive biology of many Hymenopteran species, leaving the broader role of OR-mediated olfaction in parasitoid biology largely unexplored. Given the unique subsocial behaviors of *S. guani*, including maternal care and offspring recognition, Orco-dependent olfactory signaling may play a central role in coordinating both ecological host exploitation and intraspecific social interactions.

Although the chemical ecology and behavioral repertoire of *S. guani*—including host-seeking, oviposition, and maternal care—have been studied extensively over the past two decades, molecular insight into the olfactory mechanisms underlying these behaviors has been hindered by the lack of a high-quality genome and genetic tools. This limitation has constrained a genetic-level understanding of parasitoid wasp olfaction and its potential exploitation for improved biological control strategies. Recently, we established CRISPR/Cas9-mediated gene editing in *S. guani* [54], enabling functional interrogation of

olfactory genes. Here, we integrate chromosome-level genome assembly, Hi-C–based chromatin analysis, antennal transcriptomics, electrophysiology, and CRISPR/Cas9 mutagenesis to comprehensively examine the evolutionary and functional architecture of olfaction in *S. guani*. We show that OR loci preferentially occupy interaction-rich topologically associating domain interiors, and that even OR singletons reside in chromatin environments characteristic of tandem arrays, suggesting that OR identity is intrinsically associated with duplication-permissive genomic neighborhoods. Functionally, we demonstrate that Orco-mediated olfaction is essential not only for efficient host localization and mating but also for oviposition fidelity and maternal coordination. These findings suggest that OR expansion in a subsocial parasitoid is embedded within a distinctive 3D chromatin framework and that olfactory signaling is necessary for host-seeking, mating, discriminative parasitism, and maternal care.

## Methods and Materials

### Insect rearing

The *S. guani* colony was provided by the Pest Control and Resource Utilization Laboratory at Guizhou Normal University [55]. The parasitoid wasps were reared at 25°C, with 65% relative humidity, under a 12-hour light/12-hour dark photoperiod for over 50 consecutive generations. Larvae of *M. alternatus* (host species) were purchased from Kaili, Guizhou Province, China (107.981°E, 26.566°N), and were individually maintained in 5 mL test tubes containing sawdust, stored at 4°C upon arrival.

### Genomic sequencing

30 male pupae produced parthenogenetically from a single unmated female *S. guani* were collected for genomic DNA extraction using sodium dodecyl sulfate (SDS)-based method. A SMRTbell library was constructed with PacBio SMRTbell Express Template Prep Kit 2.0 (Pacific Biosciences), and fragments ranging from 15 to 20 kb were size-selected on BluePippin System (Sage Science). The library was subsequently sequenced on PacBio Sequel II platform in Circular Consensus Sequencing (CCS) mode. Library preparation and PacBio sequencing were carried out by Novogene Co., Ltd. (Beijing, China). Sequencing yielded 25.74 Gb of PacBio high-fidelity (HiFi) reads, with an average read length of 16.55 kb and an N50 length of 16.49 kb. These high-quality HiFi reads were then used for *de novo* genome assembly.

### Transcriptomic sequencing

A total of six RNA-seq libraries were constructed for annotation. RNA samples were prepared from wasps at different developmental stages, including egg (one sample), larval (one sample), pupal (one sample), and adult (three samples) stages. The egg sample

consisted of 400 1-3-day-old eggs oviposited by mated females. The larval samples were collected from both sexually reproduced and parthenogenetic larvae at various stages: Day 1 (10 larvae), Day 3 (5 larvae), Day 5 (5 larvae), Day 7 (5 larvae) post-eclosion, as well as the spinning (5 larvae) and pre-pupal (4 larvae) stages. The pupal sample included two males and two females collected at each of the following time points: Days 3, 5, 7, 9, 11, and 13 post-pupation. For the adult stage, three distinct samples were taken: one from 5-day-old mated and unmated females (10 individuals each), one from 3-4-day-old mated and unmated males (10 individuals each), and one from maternal-caring females (10 10-15-day-old gravid females and 10 15-20-day-old post-ovipositing females). For transcriptional analysis, antennal samples were collected from 3-5-day-old adults, with three replicates for each gender. Each replicate contained 150-200 antennae.

RNA samples were extracted using PureLink RNA Mini Kit (Invitrogen). Sequencing libraries were prepared with NEBNext Ultra RNA Library Prep Kit for Illumina (E7530L, NEB), and library quality was assessed on Agilent 5400 system (Agilent). Qualified libraries were pooled and sequenced on an Illumina platform (Novaseq 6000) to generate 150 bp paired-end (PE) reads. Sample quality control, library preparation, and Illumina sequencing were performed by Novogene Co., Ltd. (Beijing, China).

## Genome assembly and annotation

### *DNA extraction and HiFi read preprocessing*

PacBio HiFi sequencing reads were filtered to remove residual sequencing adapters using HiFiAdapterFilt [56]. Adapter-trimmed reads were used for all subsequent analyses.

### *Genome assembly strategy*

Genome assembly broadly followed long-read best-practice recommendations from the Vertebrate Genome Project (VGP) and the European Reference Genome Atlas (ERGA) [57]. Assembly and preliminary analyses were performed using the Galaxy web platforms [58], supplemented by in-house validation and downstream analyses.

### *k-mer profiling and genome characterization*

To estimate genome size, heterozygosity, and repeat content, canonical 31-mers were counted from adapter-filtered HiFi reads using Meryl [59]. The resulting k-mer histogram was modeled with GenomeScope 2.0 [60], assuming diploidy (k = 31). GenomeScope parameter estimates were used to guide downstream duplication purging thresholds. (**Fig. S1**)

### *Primary contig assembly and quality assessment*

Primary contig assembly was performed with hifiasm [61] using default parameters and standard mode on trimmed HiFi reads. Assembly statistics were computed with gfastats

[62], and contigs were exported in FASTA format. K-mer–based consensus quality value (QV), completeness, and copy-number spectra were assessed using Merqury [59].

*Haplotig purging and duplication removal*

To remove redundant haplotigs and overlaps, adapter-filtered HiFi reads were mapped back to primary contigs using minimap2 [63]. Coverage statistics and depth cutoffs were estimated using purge_dups [64], guided by GenomeScope-derived parameters. Self-alignments were performed to identify duplicated regions, and purged primary contigs were recovered using the purge_dups toolkit. Assembly quality metrics were re-evaluated with Merqury following purging.

*Decontamination and taxonomic screening*

To minimize low-complexity alignment artifacts prior to taxonomic classification, the purged assembly was soft-masked using dustmasker [65], and masked bases were converted to Ns for conservative screening. Taxonomic classification was performed with Kraken2 [66] against the PlusPF database.

To further identify potential host contamination (e.g., Coleopteran sequences from parasitized hosts), we conducted translated similarity searches using DIAMOND blastx [67] against the NCBI NR database. For each scaffold, taxonomically assigned alignments were merged to calculate order-level coverage proportions. Scaffolds with disproportionately high Coleoptera-assigned coverage were flagged for manual inspection. Two contigs (ptg000246l_path_1 and ptg000081l_path_1) were removed as putative contaminants.

*Hi-C scaffolding and chromosomal assembly*

Hi-C library construction, sequencing, and scaffolding were performed by Novogene Co., Ltd. (Beijing, China) using 300 pooled *S. guani* male pupae. The Hi-C library was constructed following a previously described, standardized protocol [68]. Hi-C sequencing was performed on Illumina Novaseq 6000 platform with PE-150 strategy. Hi-C reads were mapped to the PacBio HiFi contig assembly, and chromosome-scale scaffolding was performed using the ALLHiC pipeline [69]. The resulting Hi-C contact maps were visualized and manually curated using Juicebox to correct potential misassemblies and refine scaffold orientation. This procedure produced a chromosome-level assembly consisting of 15 chromosomes, consistent with previously published karyotypes for this species [70,71], with 291.5 Mb (90.39%) of the assembled genome anchored to chromosomes.

*Structural and repeat annotation*

Structural annotation was performed using a combined evidence-based and ab initio strategy implemented by the sequencing provider. Transcript evidence was incorporated

using PASA [72], integrating RNA-seq data from eggs, larvae, and adult males and females to refine gene models. Repetitive elements were annotated with RepeatMasker.

*Functional annotation*

Functional annotation was performed in-house. Protein sequences were analyzed using InterProScan [73], eggNOG-mapper [74], Phobius [75], and SignalP [76], and functional annotations were integrated using Funannotate to assign Gene Ontology (GO) terms, Clusters of Orthologous Groups (COGs), CAZy classifications, MEROPS protease families, and BUSCO ortholog group identifiers [77].

*Assembly quality assessment*

Assembly contiguity statistics were calculated using QUAST [78] in eukaryotic mode with scaffold splitting enabled. Metrics including total assembly length, scaffold and contig N50, L50, GC content, and scaffold composition were reported (**Table S1**).

Repetitive element content was quantified from RepeatMasker annotations by parsing GFF output and aggregating total masked bases by repeat class. The proportion of the genome occupied by each repeat category was calculated relative to the final assembly length (**Table S2**).

Genome completeness was assessed using BUSCO v5 [79] against the *Arthropoda* odb12 dataset in both genome and protein modes. Genome-mode BUSCO analyses were run with MetaEuk gene prediction enabled. BUSCO completeness categories (Complete—Single Copy, Complete—Duplicated, Fragmented, and Missing) were reported as percentages of the total ortholog set (**Fig. S2**; **Table S1**).

**Mitochondrial genome identification and annotation**

The mitochondrial genome was identified from the assembled contigs using MitoFinder [80] against the *S. alternatusi* mitochondrial genome. The recovered mitochondrial contig was circularized and extracted for downstream annotation. Gene prediction was performed using MITOS2 [81] under the invertebrate mitochondrial genetic code. Predicted protein-coding genes, rRNAs, and tRNAs were manually inspected and curated in Apollo [82]. To improve visualization and prevent annotation artifacts, the circular mitochondrial genome was rotated such that no gene feature spanned the origin of the sequence. This ensured that all gene models were represented as contiguous intervals in downstream analyses and figures. The final mitochondrial annotation includes the 13 protein-coding genes, 22 tRNAs, and 2 rRNAs.

**Annotation of chemosensory receptors**

To further refine and improve chemosensory receptor gene family annotations, we implemented an iterative homology-driven refinement strategy. Here, seed HMM profiles

were constructed from curated homologous chemosensory receptor protein sequences across diverse insects by first clustering query proteins using MMseqs2 all-vs-all searches [83], determining similarity relationships using MCL [84], aligning clustered sequences using MAFFT [85], and constructing profile HMMs using HMMER [86]. These HMMs served as the initial search library for iterative homolog discovery.

The first refinement pass was performed by searching the HMM profiles against the predicted *S. guani* proteome using hmmsearch (E-value ≤ $1\times10^{-5}$). Hits were further filtered using an adaptive bitscore threshold (discarding sequences below 25% of the mean bitscore of the top 75% of hits per profile) to remove spurious matches. This step identified numerous putative chemoreceptor candidates. However, several gene models derived from PASA and identified in this search exhibited biologically implausible features (e.g., up to 34 predicted transmembrane domains), indicating fused gene models within tandem arrays. All candidate loci were therefore manually inspected and refined in Apollo using RNA-seq read alignments as supporting evidence [82]. Following manual correction, updated protein sequences were reannotated using InterProScan, eggNOG, Pfam, Phobius, and SignalP to refresh functional annotations.

To identify additional chemoreceptor genes potentially missed by PASA, a second refinement step was performed, this time searching the HMM profiles against a six-frame translation of the genome. High-scoring HSPs were chained into candidate loci based on genomic proximity and collinearity. Spaln3 was used to generate preliminary spliced gene models [87], which were subsequently refined using AUGUSTUS with profile hints derived from aligned HMM sequences [88]. Newly predicted loci were again manually curated in Apollo and functionally reannotated as described above.

A final refinement pass was conducted against the proteome as described above. Results were interpreted alongside orthology predictions generated by OrthoFinder [89] using the proteomes of *Aedes aegypti*, *Anopheles gambiae*, *Apis mellifera*, *Bombyx mori*, *Camponotus floridanus*, *Harpegnathos saltator*, *Ceratitis solmsi*, *Drosophila melanogaster*, *Nasonia vitripennis*, *Tribolium castaneum*, and *S. guani*.

Genes were classified as ORs if they were recovered in the iterative HMM-based search, contained the Pfam domain PF02949, and exhibited orthology to known insect ORs. Genes were classified as GRs if they were recovered as GR candidates, contained the Pfam domain PF08395, and exhibited orthology to known GRs. IR annotation required additional scrutiny due to shared domain architecture with ionotropic glutamate receptors (iGluRs). To avoid misclassification of canonical iGluRs, genes were classified as IRs only if they were predicted as IRs by HMMology, contained PF00060, and either clustered with antennal IRs in maximum likelihood phylogenies including known IR and iGluR sequences or exhibited orthology to established and salient IRs.

**Hi-C visualization and analysis**

To independently validate and visualize contact structure, including downstream analysis of A/B compartments and topologically associating domains (TADs), Hi-C data were reprocessed and visualized using nf-core/hic [90] and HiCExplorer [91]. Balanced contact matrices were generated at multiple resolutions (1 Mb, 640 kb, 250 kb, and 40 kb).

To restrict analyses to chromosome-level scaffolds, unplaced contigs and the mitochondrial genome were excluded using hicAdjustMatrix. Balanced .cool matrices containing only the 15 chromosomes were used for all downstream analyses.

Genome-wide contact maps were visualized at 640-kb resolution using hicPlotMatrix with log-transformed balanced contact intensities. Per-chromosome contact maps were generated at 40-kb resolution to examine fine-scale chromatin architecture. All matrices were visualized after masking low-coverage bins.

*A/B compartment identification*

Chromatin compartments were inferred from principal component analysis of the balanced Hi-C contact matrices at 250-kb resolution. The first eigenvector (PC1) was used to assign genomic bins to A and B compartments following established Hi-C compartment analysis approaches [92,93]. PC1 values were oriented by correlating eigenvector sign with gene density and GC content, such that A compartments corresponded to gene-rich, GC-variable regions. Compartment tracks were incorporated into circos visualizations for genome-wide analysis.

*TAD detection*

Topologically associating domains (TADs) were identified using hicFindTADs at 40-kb resolution with false discovery rate (FDR) correction for multiple testing. Insulation (TAD) scores were computed for each bin across chromosomes. TAD boundaries were defined based on local minima in insulation scores. Representative chromosomal regions were visualized using hicPlotTADs, integrating contact maps, insulation profiles, and gene annotations.

*Gene–TAD association metrics*

To quantify the relationship between gene class and chromatin architecture, we calculated multiple metrics for each gene, including: TAD score (local insulation score), distance from gene midpoint to TAD center, and distance from gene midpoint to nearest TAD boundary. Distances were normalized by TAD length to allow comparison across domains.

Chemosensory genes were classified as singleton or tandem array members based on genomic proximity and cluster identity, where clusters of 3 or more genes from the same receptor family located within 50kb on the same strand were considered members of a tandem array. Additional, non-chemosensory tandem arrays were identified using a

homology-aware proximity clustering approach based on OrthoFinder orthogroup assignments [89]. To focus on paralogous expansions rather than general gene clustering, orthogroups were processed to identify clusters of 3 or more homologous genes located on the same strand of the same chromosome with a maximum intergenic distance of 50kb. To prevent confounding by transposable element–related expansions, orthogroups were excluded if annotated gene products contained keywords indicative of TE-derived proteins (e.g., “transposase,” “reverse transcriptase,” “integrase,” “gag,” “pol,” “gypsy,” “copia,” or “repeat”). Chemosensory genes were excluded from this non-chemosensory tandem detection pipeline to allow independent comparison between chemosensory tandem arrays and background tandem genes. This procedure generated a genome-wide catalog of tandem arrays for non-chemosensory genes. BUSCO single-copy orthologs were identified from proteome-mode BUSCO results and used as conserved single-copy controls.

*Statistical modeling and bootstrap analysis*

To test whether chromatin organization differed systematically among gene classes, we performed linear mixed-effects modeling on gene-level TAD metrics. Analyses were conducted in Python using the statsmodels mixed linear model framework. Here, genes were classified into five groups: ORs in tandem arrays ($OR_{tan}$), OR singletons ($OR_{sin}$), non-chemosensory tandem array genes ($Other_{tan}$), gustatory and ionotropic receptor singletons (GR/IR), and BUSCO single-copy orthologs (BUSCO).

To prevent tandem arrays from artificially inflating statistical signal due to correlated neighboring genes, we collapsed tandem clusters to a single representative gene per cluster per iteration. For each bootstrap-like iteration, one gene was randomly sampled from each tandem array, ensuring that each cluster contributed equally to the model. Singleton gene classes were not collapsed.

For each response variable, we fitted the following model:

$$\text{response} \sim \text{group} + log\ (\text{TAD length}) + \text{chromosome} + (1|\text{TAD})$$

Here, response represents one of the following metrics: TAD score (insulation score), normalized distance from gene midpoint to TAD boundary, or normalized distance from gene midpoint to TAD center. Group is the fixed effect of gene class, log(TAD length) is included as a covariate to control for domain size effects, chromosome is included as a fixed effect to account for chromosome-level variation, and TAD is included as a random intercept, accounting for non-independence of genes within the same chromatin domain. Models were fit using maximum likelihood estimation.

For each model, we constructed all pairwise group contrasts using Wald tests on linear combinations of model coefficients. For each contrast (A – B), we extracted the adjusted mean difference (estimate), standard error, Wald z-statistic, and the two-sided p-value.

Benjamini–Hochberg false discovery rate (FDR) correction was applied across all pairwise comparisons within each response variable per iteration.

To assess robustness of group differences, we performed 1,000 bootstrap-like iterations. In each iteration, tandem clusters were collapsed by random selection of one gene per cluster, the mixed-effects model was refitted, all pairwise contrasts were recomputed, and FDR correction was applied. For each response and contrast, we calculated the fraction of iterations where A > B (significant), the fraction where A < B (significant), the fraction that were non-significant, a stability metric defined as the maximum of (fraction higher, fraction lower), and the median and interquartile range of effect sizes across iterations (**Table S3**). Statistical significance was defined as FDR-adjusted $P<0.05$. Directional stability was interpreted in conjunction with median effect size across bootstrap iterations. This approach ensured that statistical inference was not driven by a small number of highly correlated tandem clusters.

**Synteny analysis**

To assess large-scale chromosomal conservation between *S. guani* and *S. alternatusi* [71]. we performed whole-genome pairwise alignment using chromosome-level assemblies from both species. Prior to alignment, assemblies were filtered to retain only primary chromosomal scaffolds, excluding unplaced contigs and the mitochondrial genome. Whole-genome alignment was performed using minimap2 [63] with the asm5 preset, which is optimized for aligning closely related genome assemblies. To focus on high-confidence, macrosyntenic blocks, alignments were filtered according to the following criteria: primary alignments only (tp:A:P), minimum alignment length ≥ 50 kb, and minimum mapping quality (MAPQ) ≥ 40. These thresholds were selected to exclude short or ambiguous alignments while retaining large-scale chromosomal correspondence. Syntenic relationships were then visualized using a custom R script built on the gggenomes framework [94].

**Antennal RNA-sequencing analysis**

Differential transcript abundance was examined using bulk RNA-sequencing reads from the three biological replicates of unmated female antennae (UFA), mated female antennae (MFA), and unmated male antennae (UMA). Reads were first processed using the standardized nf-core/rnaseq pipeline [95], followed by differential expression analysis with nf-core/differentialabundance [96], which implements a DESeq2-based negative binomial generalized linear modeling framework [97]. After filtering and normalization, differential expression analysis revealed no significantly differentially abundant transcripts between UFA and MFA (data not shown), so we focused our analyses on UFA and UMA, where we identified 411 transcripts exhibiting significant sex-biased expression at an adjusted false discovery rate (FDR) < 0.05, including 202 transcripts enriched in UFA and 209 enriched in UMA.

## Single guide RNA (sgRNA) synthesis

The *Orco*-targeting sgRNA was designed using CRISPOR [98] without reference genome. The selected sgRNA sequence (GTGAACTTGATTCTGGAGAG) was then screened against the genome to ensure there were no predicted off-targets using the crisprVerse ecosystem [99]. The sgRNA was synthesized using the EnGen sgRNA Synthesis Kit (E3322S, NEB) and purified with the Monarch Spin RNA Cleanup Kit (T2030S, NEB) according to the manufacturer's instructions. sgRNA integrity and concentration were validated by gel electrophoresis and quantified using a microvolume spectrophotometer (N50, Implen).

## *S. guani* mutagenesis

The embryonic microinjection was carried out as previously described [54] with minor modifications. Newly emerged *S. guani* adults were allowed to mate for 5-10 days before mated females were collected for parasitizing *M. alternatus* larvae at a ratio of 1 wasp per 0.1 g host weight. Newly laid embryos were collected every hour and carefully aligned with fine forceps on a microscope slide for injection.

The single-guide RNA (sgRNA) and Cas9 protein were mixed at a molar ratio of 1.5:1 (320 ng/μL Cas9 + 100 ng/μL sgRNA) and incubated at room temperature for 20 minutes to assemble the ribonucleoprotein (RNP) complex. The RNP complex was kept on ice and injected into the posterior end of 0-2 hour-old embryos (G0) using a FemtoJet 4i Microinjector (Eppendorf) with borosilicate needles (BF100-50-10, Sutter), prepared with a PC-100 Vertical Puller (Narishige). Injections were conducted under a brightfield microscope equipped with a 10× objective lens (E5, Sunny Optical). After injection, the embryos were incubated on the slide under rearing conditions for 3 days.

*M. alternatus* larvae were freshly killed by freezing at -20°C for at least 3 days. The undamaged injected embryos were carefully placed on the cuticle of a dead host larva and further incubated under rearing conditions. G0 females were then allowed to mate with wild-type males and reproduce through parasitism.

For genetic validation, a mid-leg from resulting G1 females was gently dissected into 30 μL of DNA extraction buffer (1× Sodium Chloride-Tris-EDTA buffer:10 mg/mL proteinase K = 1:50) without compromising the female's reproductive capacity. Wasp genomic DNA was extracted in a thermal cycler (C1000, Bio-Rad) with the following conditions: 65°C for 50 minutes, followed by 95°C for 10 minutes. Extracted DNA samples were subjected to PCR and sequencing. G1 $Orco^{+/-}$ females carrying *Orco* gene edits were selected (**Fig. 4C**) and backcrossed to wild-type males for at least 3 generations. Subsequently, heterozygous $Orco^{+/-}$ females were crossed with $Orco^{-}$ males (a pair of wings were dissected for sequencing) to generate homozygous $Orco^{-/-}$ females (**Fig. 4C**).

## Electrophysiology

The electroantennogram (EAG) procedure followed previously described protocols with minor modifications [50]. Briefly, the head of an adult *S. guani* was excised and mounted on an EAG platform equipped with two micromanipulators and a high-impedance AC/DC preamplifier (IDAC-2, Syntech). Chlorinated silver wires in glass capillaries filled with 0.1% KCl and 0.5% polyvinylpyrrolidone were used for both reference and recording electrodes. Both antennae with the tip cut were accommodated into the recording electrode. The airflow across the preparation was maintained constant at 20 mL/s to which a stimulus pulse of 2 mL/s was delivered for 500 ms. Any change in antennal deflection induced by the stimuli or control puffs was recorded for 10 s. All compounds were dissolved in DMSO or paraffin oil to make a test solution of 10-fold dilution. An aliquot (10 μL) of a tested compound was loaded onto a filter paper strip (4 × 30 mm), which was immediately inserted into a Pasteur pipette for evaporation. Solvent alone served as control. EAG responses (ΔmV) were normalized by subtracting antennal responses to odorants by those to the solvents.

## Parasitizing assay

The testing arena is a large Petri dish (90 mm × 15 mm) containing a small Petri dish (35 mm × 10 mm) placed against its inner wall. A *M. alternatus* larva (0.45-0.55 g) was confined in the small dish to limit its movement while remaining accessible to the parasitoid wasp. Five 2-3-week-old *S. guani* females were anesthetized by brief cooling and placed in the large Petri dish, at the end distal to the small dish. The wasp reproductive behaviors were observed every 24hrs, including stinging (on-host stage, defined as female wasps mounting on the host), ovipositing (egg stage, defined as the presence of eggs), egg hatching (larval stage, defined as the presence of larvae), cocooning (pupal stage, defined as the appearance of cocoons), and emergence (adult stage, defined as the emergence of adult wasps) [100]. A brood was scored as entering a stage upon the appearance of the first individual in that stage.

During the egg and pupal stages, the number of eggs and larvae in the small Petri dish was counted every 24 hours, excluding dead individuals. Host assessment was restricted to the upper surface of the host larva, as the underside was inaccessible for reliable observation.

## Eclosion rate assay

Females were allowed to parasitize hosts under standard conditions. For each replicate, 40 eggs laid within a 24-hour period were carefully collected from the host cuticle. These eggs were monitored, and the number of successfully hatched first-instar larvae was counted to calculate the percentage eclosion rate.

## Wasp mass measurements

The body mass of newly eclosed (1-day-old) adult wasps was measured using a micro-analytical balance (GE0505S, YOKE Instrument). Measurements were taken for both sexes of wild-type and *Orco* mutant lines.

**Host-seeking assay**

Host-seeking behavior was assessed based on a previous study [101]. A single *M. alternatus* larva (0.45-0.55 g) was confined in a glass test tube (10 × 75 mm). This tube was then placed inside a 100 mL glass conical flask (108 mm in height, 40 mm in neck diameter, 66 mm in bottom diameter) sealed with a rubber plug. A mated 2-week-old *S. guani* female was then introduced to the bottom of the flask. The assay was carried out over 72 hrs and the position of the female was recorded every 12 hrs. Successful host localization was defined as the wasp's entry into the host-containing tube.

**Mating assay**

The mating assay was conducted in a cylindrical chamber (8 mm × 4 mm). Male and female wasp pupae were separated approximately 3 days before eclosion. Prior to testing, a 1-2-day-old virgin wild-type female was introduced into the arena and allowed a 1-hour acclimation period. Following this, a 2-3-day-old virgin male was placed into the arena and given 10 minutes to mate freely with the female. The mating process was recorded using a dissecting microscope (SZMN, Sunny Optical) equipped with a digital camera. Copulation was defined as the penetration of the male genitalia into the distal end of the female's abdomen.

The long-term mating assay was performed by housing a 2-day-old virgin male with five 1-2-day-old virgin females in a Petri dish (35 mm × 10 mm) for 72 hours. The male was subsequently removed. After a 5-day acclimation period, the females were provided a *M. alternatus* larva (0.45-0.55 g) in a 10 mL centrifuge tube for parasitism. As unmated females produce only male offspring via parthenogenesis, mating success was determined by assessing both the total progeny number and offspring sex ratio.

**Larval translocation assay**

The assay was conducted based on a previous study with modifications [3]. Mated female wasps were allowed to parasitize the host as described above. Offspring larvae were collected within 24 hours after detaching from the host and subsequently placed in a 60 mm × 15 mm Petri dish. In each dish, sixteen larvae were arranged in the center with a 5 mm interval. Three gravid female wasps from a different brood, actively undergoing oviposition, were then introduced. Negative controls were established in parallel without introducing female wasps.

The larval distribution was recorded after 72 hours. For each larva or cocoon, the distance to its closest neighbor was measured using ImageJ [102]. The total distance between larvae

for each replicate was used to assess translocation efficiency. The larvae were allowed to continue development, and the survival rate was calculated by dividing the number of emerging adults by the initial number of larvae (16).

## Data analysis

Statistical analyses and figure generation were performed using a combination of GraphPad Prism 8 (GraphPad Software Inc.) and custom scripting as described above.

## Results

### Chromosome-level assembly reveals compartmentalized genome architecture and LTR-driven expansion in *S. guani*

We generated a chromosome-level genome assembly for *S. guani* totaling 322.5 Mb, organized into 15 chromosomes, 50 unplaced contigs, and 1 circular mitochondrial genome (**Fig. 1A-C**; **Fig. S3**). The assembly exhibits high contiguity and completeness (**Table S1**; **Fig. S2**), with 98.4% of Arthropoda BUSCO genes identified as complete (96.2% single-copy, 2.2% duplicated), consistent with other high-quality hymenopteran assemblies [103]. Hi-C scaffolding produced strong chromosome-scale interaction patterns with minimal interchromosomal mis-joins (**Fig. 1B**; **Fig. S4**).

Comprehensive functional annotation was performed using InterProScan, eggNOG, SignalP, Phobius, and Funannotate which additionally provided CAZy, MEROPS, and Gene Ontology assignments [73–77]. However, chemosensory receptor gene families—particularly odorant receptors (ORs)—present challenges for automated annotation pipelines due to their frequent tandem duplication, high sequence divergence, and multi-exonic structure, thus requiring additional manual inspection, correction, and validation. Indeed, upon preliminary inspection, we observed systematic misannotation within OR-rich regions, including gene model fragmentation, gene fusions across tandem arrays, and aberrantly long predicted proteins containing excessive numbers of transmembrane domains. To address these limitations, manual refinement and annotation of chemosensory receptor gene families (i.e., ORs, GRs, and IRs) was performed using curated, dynamic Hidden Markov Model (HMM) profiles in a homology- and orthology-guided iterative search paradigm (see Methods and Materials). Together, these analyses yielded a richly annotated gene set suitable for evolutionary and functional interrogation.

Hi-C eigenvector decomposition revealed a clear partitioning of chromosomes into A and B compartments (**Fig. 1A, H**), consistent with patterns described across metazoans [92,93]. A compartments were enriched for gene density and displayed more heterogeneous GC content, whereas B compartments were gene-poor, exhibited relatively uniform GC composition, and were enriched in repetitive elements. These patterns are consistent with

the general association of transcriptionally active chromatin with compartment A domains [104]. Chemosensory genes, including odorant, gustatory, and ionotropic receptors, were predominantly localized within gene-dense A compartments, with ORs forming 14 tandem clusters (**Fig. 1A, H**), similar to those observed across many other hymenopteran species [35,37,105,106].

Notably, the genome of *S. guani* (322.5 Mb) is nearly double the size of the congener *S. alternatusi* (162.3 Mb), despite both species possessing 15 chromosomes (**Fig. 1D**) [71]. This size disparity appears largely attributable to the expansion of long terminal repeat (LTR) retrotransposons, which comprise 48.7% of the *S. guani* genome (**Table S2**) but only 1.42% in *S. alternatusi* [71]. Indeed, repeat annotation revealed extensive proliferation of LTR retrotransposons across the genome, particularly toward chromosomal termini (**Fig. 1A**; **Table S2**). Despite substantial differences in genome size, large-scale synteny between *S. guani* and *S. alternatusi* remains broadly conserved (**Fig. 1D**), with many chromosomes exhibiting near one-to-one correspondence. However, several chromosomes display composite linkage patterns indicative of historical fusion/fission events.

Together, these results establish a high-quality chromosome-level assembly and reveal a compartmentalized genomic landscape characterized by LTR-driven expansion and gene-dense A compartments enriched for chemosensory loci. This structural framework provides the foundation for investigating how odorant receptor expansion and chromatin organization contribute to functional and behavioral diversification.

## Expansion and tandem amplification of odorant receptors dominate the chemosensory repertoire of *S. guani*

Manual curation and phylogenetic analysis identified a total of 182 chemosensory receptors in *S. guani*, comprising one odorant receptor co-receptor (Orco), 147 tuning odorant receptors (ORs), 17 gustatory receptors (GRs), and 17 ionotropic receptors (IRs) (**Fig. 1E-H; Fig. S5**). This distribution reflects a marked predominance of ORs, a pattern widely observed in Hymenoptera and associated with the expansion of chemosensory communication and ecological specialization [35,36]. Consistent with patterns described across ants and other hymenopterans, the majority of *S. guani* ORs are organized into tandem arrays (105/148) distributed across multiple chromosomes (**Fig. 1H**).

Phylogenetic reconstruction revealed several lineage-specific expansions within *S. guani*, including diversification within the hymenopteran 9-exon OR clade, which accounts for 59.5% of all annotated ORs (88/148) (**Fig. 1E**). This clade, originally characterized in honeybees, is frequently associated with pheromone detection and chemical communication [35,38,39,106]. Notably, both *S. guani* and *N. vitripennis* exhibit independent expansions within this clade, suggesting parallel diversification within parasitoid lineages. Of note, members of the 9-exon family are found in 10 out of the 14 tandem

arrays scattered throughout the genome, including the largest tandem array of 24 genes from OR81-OR104 (**Fig. 1H**). However, there does not appear to be a meaningful bias towards tandem array formation between 9-exon (64/88 = 72.7%) and non-9-exon (41/60 = 68.3%) family members.

In contrast to the extensive OR repertoire, the GR complement of *S. guani* is modest (17 genes) and lacks clear orthologs of canonical insect $CO_2$ receptors (e.g., GR21a/GR63a in *D. melanogaster*), which are typically conserved in dipterans [19,23] (**Fig. 1F**). Reduced GR repertoires relative to Diptera are characteristic of many Hymenoptera and may reflect differences in ecological reliance on gustatory versus olfactory modalities (Robertson & Wanner, 2006).

The IR repertoire includes the conserved co-receptors IR8a, IR25a, IR76b, and IR93a, along with 11 additional tuning IRs, for a total of 17 IRs (**Fig. 1G**). These canonical co-receptors are broadly conserved across insects and function in diverse chemosensory and thermosensory pathways [18,25,26]. The relatively limited number of tuning IRs compared to ORs further underscores the dominant contribution of OR-mediated olfaction to the chemosensory system of *S. guani*.

Together, these results demonstrate that *S. guani* possesses an expanded, tandemly organized OR repertoire typical of Hymenoptera, coupled with more conserved GR and IR complements. This genomic architecture establishes odorant receptors as the principal substrate for chemosensory diversification in this species and provides the evolutionary foundation for subsequent analyses of chromatin organization and functional dependence.

**Odorant receptor loci preferentially occupy permissive 3D chromatin domains**

To determine whether tandem amplification of odorant receptors (ORs) is associated with distinct chromatin environments, we analyzed Hi-C interaction maps and topologically associating domains (TADs) at 40-kb resolution. Preliminary visual inspection revealed that large OR tandem arrays frequently coincide with regions of elevated TAD score (reduced insulation), indicative of increased interaction with neighboring genomic regions. For example, chromosome 7 contains a prominent 15-OR array residing within a domain characterized by high local contact density and diminished boundary insulation (**Fig. 2A)**.

To quantify these observations and statistically test the hypothesis that ORs reside in interaction rich chromatin domains, we compared TAD score and spatial positioning metrics across five gene classes: BUSCO single-copy orthologs (BUSCO), gustatory and ionotropic receptor singletons (GR/IR), odorant receptor singletons ($OR_{sin}$), non-OR genes in tandem arrays ($Other_{tan}$), and odorant receptors in tandem arrays ($OR_{tan}$). Here, we found that singleton loci were positioned significantly further from TAD centers and closer to TAD boundaries relative to $OR_{tan}$ and $Other_{tan}$ genes (**Fig. 2B**). Positioning near

TAD boundaries is generally associated with increased insulation and reduced cross-domain interaction [93,104], suggesting that conserved single-copy genes occupy more structurally constrained chromatin compartments.

Moreover, both $OR_{tan}$ and $Other_{tan}$ loci exhibited significantly higher TAD scores than BUSCO and GR/IR singleton genes (**Fig. 2C**), indicating localization within chromatin regions that are less insulated from neighboring domains. In contrast, BUSCO single-copy orthologs and GR/IR singleton genes were characterized by significantly lower TAD scores, consistent with residence in more insulated chromatin environments [93,104].

Interestingly, odorant receptor singletons ($OR_{sin}$) did not behave like other singleton genes. Instead, $OR_{sin}$ loci exhibited chromatin features more similar to tandem arrays than to BUSCO or GR/IR singletons. $OR_{sin}$ genes displayed significantly elevated TAD scores relative to conserved single-copy genes and were positioned closer to TAD centers and further from boundaries (**Fig. 2B, C**). Thus, even in the absence of tandem organization, OR loci preferentially reside in chromatin environments associated with increased intra-domain interaction.

These patterns were robust across 1,000 bootstrap-like iterations of mixed-effects models, with pairwise comparisons demonstrating consistent effect sizes and high significance stability (**Fig. 2B, C**; **Table S3**). Collectively, these results reveal a gene class–specific chromatin architecture in which OR loci—particularly tandem arrays but also notably OR singletons—are preferentially positioned within permissive, interaction-rich TAD interiors, whereas conserved singleton genes and other olfactory receptors occupy more insulated boundary-proximal regions (**Fig. 2D**).

## Sex-biased antennal transcription reveals female-enriched odorant receptor expression

To investigate whether genomic organization of chemosensory loci corresponds to sex-specific transcriptional regulation, we performed RNA-seq on unmated female antennae (UFA) and unmated male antennae (UMA). Differential expression analysis identified extensive transcriptional divergence between sexes, with 202 transcripts significantly enriched in females and 209 enriched in males (adjusted $P < 0.05$; **Fig. 3A**). These results indicate broad quantitative differences in antennal gene regulation.

Gene Ontology (GO) enrichment analysis revealed that female-enriched transcripts were strongly associated with olfactory and chemosensory processes, including “sensory perception of smell,” “detection of chemical stimulus involved in sensory perception of smell,” “odorant binding,” and “olfactory receptor activity” (**Fig. 3B**). Enrichment was also observed for membrane-associated categories (“plasma membrane,” “membrane”), consistent with elevated receptor expression. In contrast, male-enriched transcripts exhibited more modest and functionally distinct enrichment patterns, including “proton

transmembrane transport," "proteolysis involved in protein catabolic process," "proteasome core complex," and "V0 domain" (**Fig. 3B**), suggesting differences in metabolic and cellular regulatory processes rather than broad amplification of chemosensory signaling.

Consistent with GO enrichment results, a substantial fraction of odorant receptor (OR) transcripts was significantly more abundant in female antennae relative to males (**Fig. 3D**). In particular, two large tandem OR arrays on chromosome 8 (OR75–80 and OR81–104) exhibited strong female-biased expression, with many receptors in these clusters significantly upregulated in UFA compared to UMA (**Fig. 3C, D**).

Not all ORs exhibited female bias. A subset of receptors—including OR8, OR38, and OR117—displayed significantly higher expression in males, indicating sex-specific regulation of chemoreceptors rather than uniform amplification in females (**Fig. 3D**). By contrast, expression of the conserved OR co-receptor *Orco* did not differ significantly between sexes (adjusted $P = 0.29$), consistent with its broadly expressed role in OR signaling across olfactory sensory neurons and the expectation that sex-specific olfactory differences are primarily mediated by tuning ORs.

Antennal IR expression also differed between sexes (**Fig. 3E**). IR75u, IR93a, IR310.1, IR312, and IR313 were significantly more abundant in females, whereas IR68b, IR64a.1, and IR64a.2 were enriched in males.

Together, these results demonstrate pronounced sex-biased transcription in the antennae of *S. guani*, with female antennae characterized by coordinated upregulation of ORs, including those clusters embedded within permissive chromatin domains. This pattern suggests that genomic expansion and chromatin organization of OR loci may facilitate sex-specific amplification of olfactory signaling, potentially underlying divergent behavioral roles between males and females.

### *Orco* knockout severely impaired wasp antennal responses to semiochemicals

The expansion of the OR gene family and pronounced sex-biased differential expression of tuning ORs in *S. guani* motivated us to examine their functional roles in chemosensation and olfaction-mediated behaviors, including host-seeking, mating, and maternal care. To do so, an *Orco* mutant line was generated using CRISPR/Cas9 targeting the second exon of the *Orco* gene (**Fig. 4A**). The resulting mutant line carried a -2 bp deletion in exon 2, which was confirmed by genomic DNA sequencing (**Fig. 4B, C**).

Electroantennograms (EAGs) were performed to characterize the antennal responses of wild-type and *Orco* mutant wasps to a panel of odorants. Odorants were selected based on their ecological relevance to the wasps' behavior, as reported in previous literature [9,10,31,107–109]. Specifically, female wasps were exposed to general odorants as well as those

reported to be involved in host-seeking (**Table S4**), while males were primarily tested with female-derived odorants (**Table S5**).

Consistent with broad-scale disruption of OR-mediated olfactory signaling, *Orco* mutant females exhibited markedly reduced antennal responses across the majority of odorants tested. Compared to wild-type females, 40 out of the 44 compounds elicited reduced antennal responses in *Orco* mutants, including significant reductions in response to (+)-fenchone, 6-methyl-5-hepten-2-one, cyclohexanone, (-)-carvone, butanoic acid, α-terpineol, 1-heptanol, (E)-2-hexenol, benzaldehyde, acetophenone, eugenol, propanal, and linalool oxide (**Fig. 4D, E**). In males, overall antennal sensitivity was lower, with 22 out of 24 odorants eliciting mean responses below 0.1 mV. Although modest in absolute magnitude, such responses are consistent with EAG recordings reported in other Hymenoptera, where antennal responses often remain comparatively low despite highly developed olfactory systems [110–112]. Notably, *Orco*$^{-}$ males showed significantly reduced responses to the three odorants that elicited the highest responses in wild-type males: nonanal, benzeneacetaldehyde, and (Z)-9-tricosene (**Fig. 4F, G**).

Taken together, these results demonstrate a pronounced sex bias in antennal sensitivity and confirm that disruption of Orco dramatically impairs odor-evoked neuronal responses in *S. guani*, consistent with a central role for OR-mediated signaling in detecting ecologically relevant chemical cues.

### *Orco* mutant wasp display significant developmental and reproductive deficits

The establishment of a homozygous *Orco* null mutant strain enabled us to examine the behavioral consequences of disrupting OR-mediated olfaction. Although the homozygous mutants were viable, the line proved difficult to maintain under standard rearing conditions, prompting a detailed investigation of its reproductive fitness. Newly eclosed mutant adults did not differ in mass from their wild-type counterparts (**Fig. S6A, B**), indicating that gross morphological development was unaffected. A parasitizing assay was therefore conducted to evaluate their reproductive fitness (**Fig. 5A**). Both wild-type and *Orco*$^{-/-}$ females successfully located and mounted their hosts within 24hrs, subsequently feeding on host hemolymph and initiating oogenesis. On Day 4, oviposition commenced and continued over several days, with larvae from both genotypes beginning to hatch by Day 8. While the timing of early developmental stages was similar, pupation was markedly delayed in the *Orco*$^{-/-}$ line. By Day 20, only 16.7% of mutant offspring had pupated, whereas the majority (71.4%) of wild-type brood had pupated by Day 13 and all had pupated by Day 16. Adult emergence began on Day 27 in 71.4% of wild-type broods, whereas only 16.7% of *Orco*$^{-/-}$ broods showed emergence by Day 32 (**Fig. 5B, C**). Importantly, all seven wild-type broods successfully reproduced, yielding an average of 91.28 ± 12.60 females and 28.28 ± 4.81 males. In contrast, only 1 out of 6 *Orco*$^{-/-}$ broods produced offspring yielding a single male (**Fig. 5D**).

Given the near absence of pupal and adult stages in the *Orco*$^{-/-}$ broods, we tracked egg and larval counts every 24hrs. Although both lines initiated oviposition on Day 4, egg numbers differed significantly from Days 5-8. By Day 13, wild-type egg production ceased and cocoons formed in the wild-type broods, while *Orco*$^{-/-}$ females continued laying eggs until Day 19, indicating an extended oviposition period. Moreover, from Day 5 onward, *Orco*$^{-/-}$ females laid significantly fewer eggs, resulting in fewer larvae and an extended larval stage without subsequent cocoon formation (**Fig. 5E**).

Abnormal oviposition behavior was also observed in *Orco*$^{-/-}$ females and likely contributed to the reduced survival of eggs and larvae. Unlike wild-type females, which laid the majority of their eggs directly onto paralyzed hosts (**Fig. 5F**), *Orco*$^{-/-}$ females deposited a substantial portion of their eggs on the Petri dish surface, peripheral to the host (**Fig. 5G**) or, in some cases, within excretory matter (**Fig. 5H**). This off-host oviposition resulted in larval developmental failure (**Fig. 5I**). Analysis at the time points with maximum egg count (Day 7 for the wild-type brood and Day 9 for the *Orco*$^{-/-}$ brood) revealed a significant preference for on-host egg-laying in wild-type females that was absent in *Orco*$^{-/-}$ females (**Fig. 5J**). Furthermore, *Orco*$^{-/-}$ females frequently laid eggs on top of existing eggs (**Fig. 5K**) or larvae (**Fig. 5L**), which likely induced larval cannibalism upon hatching (**Fig. 5K**). Importantly, egg eclosion rates did not differ significantly between genotypes (**Fig. S7**), indicating that reduced reproductive success in *Orco*$^{-/-}$ females is not due to impaired egg viability but instead likely results from abnormal oviposition behavior.

## *Orco* mutant wasp exhibited considerable host-seeking deficits

Given the severe reproductive deficits observed in *Orco*$^{-/-}$ females, we next investigated whether disruption of OR-mediated signaling also impaired host-seeking behavior. In the initial assay, females were placed in a simplified two-dimensional arena with a constrained host (**Fig. 5A**). In this context, the duration of the pre-oviposition period was the same between wild-type and mutant females (**Fig. 5B, C**). Because hosts were readily encountered in this simplified arena, however, this metric may not accurately reflect host-seeking ability. Therefore, we further evaluated host-seeking behavior in a more naturalistic three-dimensional scenario. In this assay, a single female was introduced into an arena and allowed to search for a host restrained within a test tube (**Fig. 5M**). Successful host localization was defined as the female entering the tube (**Fig. 5N**). Over a 72-hour observation period, 100% wild-type females successfully locate the host, whereas only 24% *Orco*$^{-/-}$ females did so (**Fig. 5O**). The success rate plateaued within the first 48 hours (**Fig. 5O**), indicating that Orco is essential for efficient host localization under ecologically relevant conditions.

## *Orco* mutant wasp demonstrated dramatic mating deficits

Given the severe reproductive and host-seeking failures observed in *Orco* mutants, we next asked whether disruption of OR-mediated signaling also impaired mating behavior. To do so, we conducted mating assays using virgin adults. Individual virgin males from both wild-type and *Orco* mutant strains were paired with a single virgin wild-type female in a confined mating chamber (**Fig. 6A**). In wild-type pairings, 9 out of 10 wild-type males successfully mated within 10 mins, with a mean pre-copulatory latency of 146 ± 58 seconds. These males exhibited typical copulation behaviors, including antennal tapping (**Fig. 6B**), mounting (**Fig. 6C**), and genitalia insertion (**Fig. 6D**). In contrast, only 1 out of 10 *Orco*$^{-}$ males achieved successful copulation, indicating a severe impairment in mating efficiency (**Fig. 6E**).

To further investigate whether the *Orco* mutation impairs fecundity at the population level, we conducted a long-term mating assay in which individual virgin males were housed with five virgin females for 72 hours (**Fig. 6F**). The subsequent offspring production, including total progeny number and sex ratio, was quantified and compared between genotypes. The results showed that both the number of offspring (**Fig. 6G**) and their sex ratio (**Fig. 6H**) were not significantly different wild-type and *Orco*$^{-}$ males. Therefore, despite the pronounced mating deficits, colony maintenance of the *Orco* mutant strain remained feasible by extending the mating exposure period to ensure sufficient fertilization of females.

## ***Orco* mutant wasp revealed dramatic maternal care deficits**

In light of *S. guani*'s unique maternal care system, we next tested whether disruption of OR signaling impaired this specialized social behavior. To quantify maternal care independently of reproduction, we introduced females as "stepmothers" to groups of late-instar larvae (**Fig. 7A**). Maternal care capacity was assessed by measuring the nearest-neighbor distances after 72 hours, with reduced distances indicating enhanced clustering behavior.

Compared to the negative control (larvae alone, 117.50 ± 7.44 mm; **Fig. 7B, C**), the presence of wild-type females significantly increased larval clustering (63.92 ± 5.50 mm; **Fig. 7B, D**). In contrast, the *Orco*$^{-/-}$ females produced clusters more comparable to the negative control (92.98 ± 8.42 mm; **Fig. 7B, E**). Moreover, the presence of *Orco*$^{-/-}$ females appeared to be detrimental to the larvae, resulting in significantly reduced larval survival rates (15.63 ± 6.60%) compared to broods reared with wild-type females (77.68 ± 2.68%) or even those in the negative control (91.07 ± 4.06%; **Fig. 7F**).

Intriguingly, in all replicates, *Orco*$^{-/-}$ females exhibited abnormal egg-laying behavior, characterized by oviposition on one or more conspecific larvae (**Fig. 7G**) and occasionally the resulting pupae (**Fig. 7H**). This intraspecific oviposition led to larval/pupal death due to subsequent cannibalism by the emerging offspring (**Fig. 7G**). No such conspecific egg-laying behavior was observed in wild-type females.

Cocoon formation was also affected by maternal care. In the absence of maternal care, larval cocoons formed primarily along the margins of the Petri dish (20.54 ± 5.05%) rather than in clustered groups (10.71 ± 3.26%; **Fig. 7C, I**). As expected, wild-type females significantly enhanced cocoon formation by actively gathering the larvae (**Figure 7D, I**); under their care, grouped cocoons (66.96 ± 4.03%) significantly outnumbered marginal ones (5.36 ± 2.87%). Conversely, the presence of *Orco*$^{-/-}$ females severely impaired cocoon formation (15.62 ± 6.80% in total), likely due to high larval mortality prior to spinning (**Fig. 7E, I**). Across all experimental conditions, successful cocoon formation occurred predominantly in either grouped or marginal configurations (**Fig. 7J**).

## Discussion

We present a chromosome-level genome assembly for *S. guani* that reveals a highly organized and compartmentalized nuclear architecture shaped by extensive lineage-specific repeat expansion. The 322.5 Mb assembly, organized into 15 chromosomes with strong Hi-C support and high BUSCO completeness (98.4% complete Arthropoda orthologs), provides a robust and essential resource for detailed investigations into this important biocontrol agent. The high contiguity and chromosomal integrity observed here are consistent with current best-practice long-read assemblies in Hymenoptera and establish a reliable foundation for analyses of three-dimensional genome organization and functional genomic architecture.

### LTR retrotransposon proliferation drives genome expansion

A striking feature of the *S. guani* genome is its nearly two-fold expansion relative to the closely related *S. alternatusi*, despite conservation of chromosome number. This expansion is overwhelmingly attributable to long terminal repeat (LTR) retrotransposon proliferation, which constitutes 48.7% of the genome in *S. guani* compared to only 1.42% in *S. alternatusi*. LTR amplification is a well-documented driver of genome size expansion in insects and other eukaryotes [113,114], suggesting lineage-specific transposable element proliferation as a primary contributor to genome enlargement in *S. guani*. The enrichment of LTR elements toward chromosomal termini in *S. guani* further suggests spatially non-uniform TE dynamics, potentially reflecting differences in recombination rate or chromatin state across chromosomal landscapes. In addition to LTR expansion, several chromosomes also display composite linkage patterns, suggesting that fusion/fission events have occurred since divergence of the two species.

### OR expansion is embedded in active and structurally permissive chromatin domains

Our analyses reveal that the chemosensory repertoire of *S. guani* is overwhelmingly dominated by ORs, which comprise nearly 90% of identified chemosensory genes. Within this compartmentalized landscape, chemosensory receptor genes— ORs, GRs,

and IRs—are preferentially localized to gene-dense A compartments. ORs, in particular, frequently occur in tandem clusters embedded within these active domains. The enrichment of chemosensory loci within A compartments is consistent with their transcriptionally dynamic roles in sensory tissues and parallels observations in other hymenopteran genomes where OR expansions occur in clustered, gene-rich regions [35,37,105,106].

A defining feature of the *S. guani* OR repertoire is its extensive organization into tandem arrays distributed across multiple chromosomes. Tandem amplification is a hallmark of hymenopteran OR evolution and has recently been shown to play a fundamental role in the transcriptional regulation of ORs [44]. The presence of multiple lineage-specific expansions within *S. guani*, including diversification within the hymenopteran 9-exon OR clade, suggests ongoing adaptive radiation. The 9-exon clade has been repeatedly implicated in pheromone detection and social chemical communication in ants and other Hymenoptera [38,39]. The independent expansion of this clade in both *S. guani* and *Nasonia vitripennis* indicates parallel evolutionary trajectories within parasitoid wasps, potentially reflecting adaptation to host-associated chemical cues or species-specific communication systems. In contrast, the gustatory receptor (GR) and ionotropic receptor (IR) complements are comparatively modest. The absence of canonical $CO_2$ receptor orthologs and the limited number of tuning IRs reinforce the interpretation that OR-mediated olfaction constitutes the principal axis of chemosensory diversification in *S. guani*.

Taken together, these findings establish OR genes as the primary genomic substrate for sensory innovation in *S. guani*. However, the expansion of ORs is not merely a matter of gene number. Our analyses indicate that OR diversification is embedded within a distinctive three-dimensional chromatin architecture. Indeed, a central finding of this study is that OR loci occupy quantitatively different chromatin environments relative to other singleton genes. Tandem arrays, including tandem arrays of ORs, are preferentially located within TADs characterized by elevated TAD scores and reduced insulation from neighboring regions. These domains exhibit higher local interaction frequencies, suggesting that OR arrays reside within chromatin neighborhoods that are structurally permissive and interaction-rich.

In contrast, conserved single-copy orthologs (BUSCO genes) and singleton GR/IR loci are positioned closer to TAD boundaries and display lower TAD scores, consistent with residence in more insulated chromatin contexts. TAD boundaries are frequently enriched for architectural proteins and regulatory insulation elements that constrain enhancer–promoter interactions [115–117]. The boundary-proximal positioning of conserved singleton genes may therefore reflect selective pressure to maintain regulatory stability and minimize ectopic interactions. On the other hand, the spatial packing of tandem arrays along the TAD may inherently constrain their position towards the center. Our analysis at

least partially mitigates this by normalizing by TAD length and sampling one representative gene per tandem array, but it does not fully eliminate all possible effects of the array span.

The most provocative feature of our dataset, however, is that OR singletons do not conform to the same pattern as other singleton loci but instead exhibit chromatin features more similar to tandem arrays. OR singletons are preferentially positioned toward TAD interiors, display elevated TAD scores, and are situated further from insulating boundaries. Moreover, in light of OR singletons showing significant positional bias towards the interior of TADs, these patterns are unlikely to be explained solely by the geometric packing constraints of extended arrays.

One intriguing interpretation is that OR loci are preferentially embedded within "evolvable neighborhoods": chromatin domains that are both transcriptionally permissive (A-compartment enriched) and structurally interaction-rich (high TAD score). Comparative genomics demonstrates that selection on 3D genome organization is often strongest at TAD boundaries, where rearrangements and deletions can be constrained or selected against [118–120]. Moreover, strong boundaries may be protected from loss and can be co-duplicated with regulatory elements under some contexts [121]. In contrast, interior regions of domains may provide greater tolerance for local structural remodeling. Such environments could, in principle, facilitate duplication via unequal crossing over, replication slippage, or local rearrangements, thereby accommodating tandem amplification while also supporting coordinated access to regulatory programs.

Distinguishing whether such chromatin contexts predispose loci to expansion or instead reflect the long-term accumulation of expanded families will require cross-species Hi-C comparisons. Nevertheless, these findings raise the possibility that three-dimensional genome organization itself constitutes an evolutionary substrate shaping the diversification of sensory gene families.

**Sex-biased antennal expression reveals coordinated female upregulation of tandem OR arrays**

While genomic expansion establishes the potential for sensory diversification, transcriptional regulation determines how this repertoire is deployed *in vivo*. Our RNA-seq analysis of unmated male and female antennae revealed pronounced sex-biased transcription across the chemosensory landscape. Approximately 400 genes exhibited significant differential expression, with female antennae showing strong enrichment for categories directly related to olfactory perception, odorant binding, and olfactory receptor activity. In contrast, male-biased transcripts were enriched primarily in metabolic and proteasomal pathways, suggesting more modest chemosensory specialization.

The most striking transcriptional asymmetry involved odorant receptors. Large tandem arrays on chromosome 8 (OR75–80 and OR81–104) displayed coordinated upregulation in females relative to males. These arrays reside within high TAD-score domains characterized by elevated intra-domain interaction, suggesting that their three-dimensional chromatin context may facilitate coordinated, sex-specific transcriptional activation. The concentration of female-biased ORs within these clusters implies that tandem organization and chromatin positioning may enable synchronized regulation of tandem arrays in response to sex-specific ecological demands.

**Electrophysiological analysis reveals Orco-dependent and -independent olfactory pathways.**

Our EAG data provide foundational physiological evidence that *Orco* mutation severely impairs peripheral olfactory function. Consistent with previous reports [10], antennal responses in wild-type females to many host- and pine tree-derived volatiles were of moderate amplitude. Across the odor panel, *Orco* mutants showed consistently attenuated antennal responses relative to wild-type, indicating a global reduction in odor-evoked sensitivity rather than a defect limited to a small subset of ligands. Indeed, a subset of compounds including (+)-fenchone and α-terpineol were significantly diminished in *Orco*$^{-/-}$ females, and the directionality of response reduction was widespread across the various odors tested, supporting the conclusion that Orco-dependent OR complexes provide the dominant contribution to volatile detection in this species. In males, this phenotype was even more pronounced, with *Orco*$^{-}$ mutants showing significant reductions in response to key putative pheromonal compounds like nonanal and (Z)-9-tricosene. (Z)-9-tricosene has been shown to be a sex pheromone is multiple insect species [122–124], and nonanal has been previously identified as a male parasitoid wasp attractant in a previous Orco study of a braconid wasp, *Microplitis mediator* [125]. Residual responses to select volatiles in *Orco* mutants, such as butanoic acid, are consistent with Orco-independent chemosensory channels—most plausibly ionotropic receptors and/or gustatory receptors—contributing to detection of specific chemical classes. Together, these electrophysiological data provide a mechanistic explanation for the behavioral phenotypes reported below and support a model in which OR-mediated signaling is the principal, but not exclusive, pathway for odor detection in *S. guani*.

**Orco-mediated olfaction is required for host localization in complex environments**

The behavioral impact of *Orco* disruption of host-seeking behavior depended on search geometry and cue availability. In a simplified two-dimensional arena, *Orco*$^{-/-}$ females successfully located and initiated parasitism, likely due to close-range gustatory, tactile, and visual cues which can be encountered through random patrols of the local environment. However, when host-seeking required navigation across a larger, more complex three-dimensional space, the successful localization of hosts in mutant females

was significantly impaired. This context dependence indicates that Orco-dependent detection of volatile kairomones is dispensable for near-field host encounter but necessary for efficient host search in a 3D space. These results support a model in which relatively high-volatility plant- and host-associated odorants attract wasps over longer distances, while low volatility tastants, tactile stimuli, and visual features mediate close-range recognition [126].

**Mating efficiency, but not ultimate reproductive output, requires Orco**

*Orco*$^{-}$ males showed significantly reduced copulation efficiency in a short-term assay, likely due to impaired detection of female-emitted volatile cues. However, when housed with females for a prolonged period, their mating success reached levels comparable to wild-type males. This pattern indicates that Orco-dependent olfaction accelerates mate localization under time-limited conditions, whereas sustained co-habitation may permit compensation through stochastic encounters and close-range cues.

**Orco-dependent signaling enforces oviposition fidelity**

The most profound phenotype was the catastrophic reproductive failure of *Orco*$^{-/-}$ females, stemming from a complete breakdown in oviposition site selection. Mutants laid eggs indiscriminately on non-host substrates (including on waste piles) and, most strikingly, on conspecific eggs and larvae. This loss of oviposition fidelity indicates that Orco is required for females to recognize the specific chemical signatures of a suitable egg-laying site and suppress oviposition on unsuitable—or socially catastrophic—substrates.

Across insects, OR-mediated signaling contributes to reproductive behavior, oviposition decisions, site preferences, and egg production [42,53,127–131], paralleling the indiscriminate egg placement we observe here. In ants and the parasitoid wasp *Leptopilina*, Orco regulates egg-laying number [42,53]. Interestingly, in moths and mosquitoes, *Orco* null mutants lose preference for optimal oviposition site [127,132], mirroring our findings.

Moreover, this defect may also relate to host-marking pheromones, which are secreted by female parasitoid wasps to regulate conspecific oviposition. Here, female parasitoids secrete host-marking pheromones with their oviducts on the host or host-associated plants to induce avoidance of conspecific wasps [133–137]. Although host-marking pheromones in the subsocial *Sclerodermus* wasps remain cryptic, gravid females secrete a slime that aids egg attachment [2], which may plausibly release attractive, rather than deterrent, marking pheromones to coordinate gregarious parasitism. In this light, *Orco* mutant females may fail to integrate volatile and contact cues that normally specify “host”, “brood”, and “non-target” oviposition sites, leading to indiscriminate oviposition and intraspecific egg-laying.

**Orco is required for maternal care**

These same recognition failures extend into subsocial behavior. Maternal care, including larval translocation, aggregation, and the promotion of cocoon spinning, is a defining behavior in *Sclerodermus* wasps. Females perform antennal tapping before translocating larvae, a process likely involving olfactory and tactile recognition and discrimination of conspecific brood [3]. Here, our assays demonstrate that olfaction is necessary for this behavior. In contrast to wild-type females aggregating larvae and promoting cocoon formation, *Orco*$^{-/-}$ females failed to do so and, strikingly, laid eggs on conspecific larvae and pupae. This indicates a severe breakdown in intraspecific recognition.

A recent study suggests that ovarian development is suppressed during maternal care in *S. guani* [138], indicating a behavioral shift from reproduction to maternal care. In ants, *Orco* mutants similarly display nursing deficits and impaired task group transitions [41]. Our data suggest that Orco-dependent olfaction is potentially central to this shift in *S. guani*. We therefore propose that OR signaling is necessary for discriminative parasitism and subsocial maternal care.

In addition, our assays have identified a key factor for cocoon spinning. The larvae require a support point for stable cocoon formation, which can be either the edge of the Petri dish or, most importantly in nature, other larvae. Maternal aggregation thus directly structures the developmental environment, linking Orco-dependent recognition to brood to offspring survival.

## Limitations and Future Directions

Three limitations shape interpretation and motivate next steps. First, our Hi-C and TAD analyses reflect the assayed tissue and developmental state. While domain structure is often broadly conserved across cell types, boundary strength and sub-TAD features can vary [118,119,139,140]. Future work using higher-resolution contact maps (e.g., Micro-C) and sensory-tissue/cell-type-specific assays would clarify whether OR neighborhoods exhibit specialized subdomain organization in antennae. Second, to directly test the “chromatin predisposition” hypothesis, comparative datasets across insect species could determine whether OR gains repeatedly arise in similar chromatin contexts, and whether expanded loci measurably reshape local insulation landscapes through time. Third, Orco disruption can have developmental and neural consequences in some insects, complicating the partitioning of acute sensory loss versus developmental rewiring [41–43]. Conditional or temporally controlled manipulations would strengthen causal inference about adult behavioral gating.

## References

1. Yang, Z., Wang, X., Cao, L., Yao, Y., and Tang, Y. (2014). Re-description of *Sclerodermus guani* and revision of the genus (Hymenoptera: Bethylidae) in China. Chinese J. Biol. Control *30*, 1–12.

2. He, K., Xu, Z., and Dai, P. (2006). The parasitizing behavior of *Scleroderma guani* Xiao *et* Wu (Hymenoptera: Bethylidae) wasps on *Tenebrio molitor* pupae. Acta Entomol. Sin. *49*, 454–460.

3. Wu, S., Xu, F., Li, B., and Meng, L. (2013). Initiation and rhythm of larva-translocation behavior during maternal care in an ectoparasitoid *Sclerodermus guani* (Hymenoptera: Bethylidae). Acta Entomol. Sin. *56*, 392–397.

4. Zhang, W., Sun, X., Qu, A., and Liu, Y. (2004). The oviposition behaviour of *Scleroderma guani* Xiao *et* Wu. Nat. Enemies Insects *26*, 28–33.

5. Wu, S., Zhou, Z., Peng, S., Li, Y., Li, B., and Meng, L. (2017). Influence of foundresss-offspring kinship on maternal care behavior and offspring developmental performance in *Sclerodermus guani* (Hymenoptera: Bethylidae). Acta Entomol. Sin. *60*, 1041–1045.

6. Huang, W., and Li, L. (2017). Maternal care improves offspring developmental performance in *Scleroderma guani* (Hymenoptera: Bethylidae). Acta Entomol. Sin. *60*, 441–449.

7. Tang, X., Meng, L., Kapranas, A., Xu, F., Hardy, I.C.W., and Li, B. (2014). Mutually beneficial host exploitation and ultra-biased sex ratios in quasisocial parasitoids. Nat. Commun. *5*, 4942.

8. Hu, Z., Zhao, X., Li, Y., Liu, X., and Zhang, Q. (2012). Maternal care in the parasitoid *Sclerodermus harmandi* (Hymenoptera: Bethylidae). PLoS One *7*, e51246. https://doi.org/10.1371/journal.pone.0051246.

9. Li, Z., Li, B., Hu, Z., Michaud, J.P., Dong, J., Zhang, Q., and Liu, X. (2015). The ectoparasitoid *Scleroderma guani* (Hymenoptera: Bethylidae) uses innate and learned chemical cues to locate its host, larvae of the pine sawyer *Monochamus alternatus* (Coleoptera: Cerambycidae). Florida Entomol. *98*, 1182–1187.

10. Li, L., Liu, Z., and Sun, J. (2015). Olfactory cues in host and host-plant recognition of a polyphagous ectoparasitoid *Scleroderma guani*. BioControl *60*, 307–316.

11. Wang, S.Y., Hackney Price, J., and Zhang, D. (2019). Hydrocarbons catalysed by TmCYP4G122 and TmCYP4G123 in *Tenebrio molitor* modulate the olfactory response of the parasitoid *Scleroderma guani*. Insect Mol. Biol. *28*, 637–648.

12. Yu, Q., Li, S., Kong, Y.J., Sun, Z.X., Cao, D.D., and Wei, J.R. (2024). Host preference and mortality caused by the parasitoid *Sclerodermus guani* on different cerambycid species. BioControl *69*, 611–621.

13. Luo, L., and Li, L. (2018). Mating behavior of *Sclerodermus guani* (Hymenoptera:

Bethylidae). Acta Entomol. Sin. *61*, 604–612.

14. Li, X., Lu, D., Liu, X., Zhang, Q., and Zhou, X. (2011). Ultrastructural characterization of olfactory sensilla and immunolocalization of odorant binding and chemosensory proteins from an ectoparasitoid *Scleroderma guani* (Hymenoptera: Bethylidae). Int. J. Biol. Sci. *7*, 848–868.

15. Chen, Y., Wang, C., Yu, X., Wang, B., and Liu, Z. (2025). A comparative morphological study of the ultrastructure of antennal sensilla in *Sclerodermus guani* (Hymenoptera: Bethylidae). Insects *16*, 547.

16. Clyne, P.J., Warr, C.G., Freeman, M.R., Lessing, D., Kim, J., and Carlson, J.R. (1999). A novel family of divergent seven-transmembrane proteins: Candidate odorant receptors in *Drosophila*. Neuron *22*, 327–338.

17. Clyne, P.J., Warr, C.G., and Carlson, J.R. (2000). Candidate taste receptors in *Drosophila*. Science *287*, 1830–1834.

18. Benton, R., Vannice, K.S., Gomez-Diaz, C., and Vosshall, L.B. (2009). Variant ionotropic glutamate receptors as chemosensory receptors in Drosophila. Cell *136*, 149–162.

19. Jones, W.D., Cayirlioglu, P., Grunwald Kadow, I., and Vosshall, L.B. (2007). Two chemosensory receptors together mediate carbon dioxide detection in *Drosophila*. Nature *445*, 86–90.

20. Dahanukar, A., Foster, K., Van der Goes van Naters, W.M., and Carlson, J.R. (2001). A Gr receptor is required for response to the sugar trehalose in taste neurons of *Drosophila*. Nat. Neurosci. *4*, 1182–1186.

21. Chyb, S., Dahanukart, A., Wickens, A., and Carlson, J.R. (2003). *Drosophila* Gr5a encodes a taste receptor tuned to trehalose. Proc. Natl. Acad. Sci. U. S. A. *100*, 14526–14530.

22. Weiss, L.A., Dahanukar, A., Kwon, J.Y., Banerjee, D., and Carlson, J.R. (2011). The molecular and cellular basis of bitter taste in *Drosophila*. Neuron *69*, 258–272.

23. Kwon, J.Y., Dahanukar, A., Weiss, L.A., and Carlson, J.R. (2007). The molecular basis of CO2 reception in *Drosophila*. Proc. Natl. Acad. Sci. U. S. A. *104*, 3574–3578.

24. Robertson, H.M., and Kent, L.B. (2009). Evolution of the gene lineage encoding the carbon dioxide receptor in insects. J. Insect Sci. *9*, 19.

25. Croset, V., Rytz, R., Cummins, S.F., Budd, A., Brawand, D., Kaessmann, H., Gibson, T.J., and Benton, R. (2010). Ancient protostome origin of chemosensory ionotropic glutamate receptors and the evolution of insect taste and olfaction. PLoS Genet. *6*, e1001064.

26. Knecht, Z.A., Silbering, A.F., Cruz, J., Yang, L., Croset, V., Benton, R., and Garrity, P.A. (2017). Ionotropic receptor-dependent moist and dry cells control

hygrosensation in *Drosophila*. Elife *6*, e26654.

27. Larsson, M.C., Domingos, A.I., Jones, W.D., Chiappe, M.E., Amrein, H., and Vosshall, L.B. (2004). Or83b encodes a broadly expressed odorant receptor essential for *Drosophila* olfaction. Neuron *43*, 703–714.

28. Benton, R., Sachse, S., Michnick, S.W., and Vosshall, L.B. (2006). Atypical membrane topology and heteromeric function of *Drosophila* odorant receptors in vivo. PLoS Biol. *4*, 240–257.

29. Zhao, J., Chen, A.Q., Ryu, J., and del Mármol, J. (2024). Structural basis of odor sensing by insect heteromeric odorant receptors. Science *384*, 1460–1467.

30. Wang, Y., Qiu, L., Wang, B., Guan, Z., Dong, Z., Zhang, J., Cao, S., Yang, L., Wang, B., Gong, Z., et al. (2024). Structural basis for odorant recognition of the insect odorant receptor OR-Orco heterocomplex. Science *384*, 1453–1460.

31. Huang, G., Liu, Z., Gu, S., Zhang, B., and Sun, J. (2023). Identification and functional analysis of odorant-binding proteins of the parasitoid wasp *Scleroderma guani* reveal a chemosensory synergistic evolution with the host *Monochamus alternatus*. Int. J. Biol. Macromol. *249*, 126088.

32. Huang, G., Liu, Z., Zhang, B., and Sun, J. (2025). Entomopathogen-associated volatiles enable parasitoid host discrimination via selective odorant receptor activation. Entomol. Gen. *45*, 1135–1145.

33. Legan, A.W., Jernigan, C.M., Miller, S.E., Fuchs, M.F., and Sheehan, M.J. (2021). Expansion and accelerated evolution of 9-exon odorant receptors in *Polistes* paper wasps. Mol. Biol. Evol. *38*, 3832–3846.

34. McKenzie, S.K., and Kronauer, D.J.C. (2018). The genomic architecture and molecular evolution of ant odorant receptors. Genome Res. *28*, 1757–1765.

35. Robertson, H.M., and Wanner, K.W. (2006). The chemoreceptor superfamily in the honey bee, *Apis mellifera*: Expansion of the odorant, but not gustatory, receptor family. Genome Res. *16*, 1395–1403.

36. Zhou, X., Rokas, A., Berger, S.L., Liebig, J., Ray, A., and Zwiebel, L.J. (2015). Chemoreceptor evolution in Hymenoptera and its implications for the evolution of eusociality. Genome Biol. Evol. *7*, 2407–2416.

37. Engsontia, P., Sangket, U., Robertson, H.M., and Satasook, C. (2015). Diversification of the ant odorant receptor gene family and positive selection on candidate cuticular hydrocarbon receptors. BMC Res. Notes *8*, 380.

38. Slone, J.D., Pask, G.M., Ferguson, S.T., Millar, J.G., Berger, S.L., Reinberg, D., Liebig, J., Ray, A., and Zwiebel, L.J. (2017). Functional characterization of odorant receptors in the ponerine ant, *Harpegnathos saltator*. Proc. Natl. Acad. Sci. U. S. A. *114*, 8586–8591.

39. Pask, G.M., Slone, J.D., Millar, J.G., Das, P., Moreira, J.A., Zhou, X., Bello, J., Berger, S.L., Bonasio, R., Desplan, C., et al. (2017). Specialized odorant receptors

in social insects that detect cuticular hydrocarbon cues and candidate pheromones. Nat. Commun. *8*, 297.

40. McKenzie, S.K., Fetter-Pruneda, I., Ruta, V., and Kronauer, D.J.C. (2016). Transcriptomics and neuroanatomy of the clonal raider ant implicate an expanded clade of odorant receptors in chemical communication. Proc. Natl. Acad. Sci. U. S. A. *113*, 14091–14096.

41. Yan, H., Opachaloemphan, C., Mancini, G., Yang, H., Gallitto, M., Mlejnek, J., Leibholz, A., Haight, K., Ghaninia, M., Huo, L., et al. (2017). An engineered orco mutation produces aberrant social behavior and defective neural development in ants. Cell *170*, 736-747.e9.

42. Trible, W., Olivos-Cisneros, L., McKenzie, S.K., Saragosti, J., Chang, N.C., Matthews, B.J., Oxley, P.R., and Kronauer, D.J.C. (2017). orco mutagenesis causes loss of antennal lobe glomeruli and impaired social behavior in ants. Cell *170*, 727-735.e10.

43. Ferguson, S.T., Park, K.Y., Ruff, A.A., Bakis, I., and Zwiebel, L.J. (2020). Odor coding of nestmate recognition in the eusocial ant *Camponotus floridanus*. J. Exp. Biol. *223*, jeb215400.

44. Glotzer, G.L., Pastor, P.D.H., and Kronauer, D.J.C. (2025). Transcriptional interference gates monogenic odorant receptor expression in ants. Curr. Biol. *35*, 5033-5047.e5.

45. Spielmann, M., Lupiáñez, D.G., and Mundlos, S. (2018). Structural variation in the 3D genome. Nat. Rev. Genet. *19*, 453–467.

46. Kim, K., Eom, J., and Jung, I. (2019). Characterization of structural variations in the context of 3d chromatin structure. Mol. Cells *42*, 512–522.

47. Pancaldi, V. (2021). Chromatin network analyses: Towards structure-function relationships in epigenomics. Front. Bioinforma. *1*, 742216.

48. Long, T., Mohapatra, P., Ballou, S., and Menuz, K. (2024). Odorant receptor co-receptors affect expression of tuning receptors in *Drosophila*. Front. Cell. Neurosci. *18*, 1390557.

49. Cooke, M.M., Chembars, M.S., and Pitts, R.J. (2025). The dysregulation of tuning receptors and transcription factors in the antennae of Orco and Ir8a mutants in *Aedes aegypti* suggests a chemoreceptor regulatory mechanism involving the MMB/dREAM complex. Insects *16*, 638.

50. Yao, H., Qi, Q., Gou, D., Liang, S., Ferguson, S.T., Li, M., Zhang, H., Ye, Z., and Liu, F. (2025). Unveiling the developmental dynamics and functional role of Odorant Receptor Co-receptor (Orco) in *Aedes albopictus*: A novel mechanism for regulating odorant receptor expression. PLoS Negl. Trop. Dis. *19*, e0013753.

51. Salvesen, H.A., and Dearden, P.K. (2025). Genome editing in hymenoptera. Insect Biochem. Mol. Biol. *180*, 104300.

52. Chen, Z., Traniello, I.M., Rana, S., Cash-Ahmed, A.C., Sankey, A.L., Yang, C., and Robinson, G.E. (2021). Neurodevelopmental and transcriptomic effects of CRISPR/Cas9-induced somatic orco mutation in honey bees. J. Neurogenet. *35*, 320–332.

53. Zhang, Q., Chen, J., Wang, Y., Lu, Y., Dong, Z., Shi, W., Pang, L., Ren, S., Chen, X., and Huang, J. (2023). The odorant receptor co-receptor gene contributes to mating and host-searching behaviors in parasitoid wasps. Pest Manag. Sci. *79*, 454–463.

54. Ye, Z., Fan, G., Wei, Y., Li, L., and Liu, F. (2025). CRISPR/Cas9-mediated germline mutagenesis in the subsocial parasitoid wasp, *Sclerodermus guani*. Insect Mol. Biol. *34*, 939–947.

55. Wei, Y., Li, L., Pan, S., Liu, Z., Fan, J., and Tang, M. (2023). Adaptive reproductive strategies of an ectoparasitoid *Sclerodermus guani* under the stress of its entomopathogenic fungus *Beauveria bassiana*. Insects *14*, 320.

56. Sim, S.B., Corpuz, R.L., Simmonds, T.J., and Geib, S.M. (2022). HiFiAdapterFilt, a memory efficient read processing pipeline, prevents occurrence of adapter sequence in PacBio HiFi reads and their negative impacts on genome assembly. BMC Genomics *23*, 157.

57. Larivière, D., Abueg, L., Brajuka, N., Gallardo-Alba, C., Grüning, B., Ko, B.J., Ostrovsky, A., Palmada-Flores, M., Pickett, B.D., Rabbani, K., et al. (2024). Scalable, accessible and reproducible reference genome assembly and evaluation in Galaxy. Nat. Biotechnol. *42*, 367–370.

58. Afgan, E., Baker, D., Batut, B., Van Den Beek, M., Bouvier, D., Ech, M., Chilton, J., Clements, D., Coraor, N., Grüning, B.A., et al. (2018). The Galaxy platform for accessible, reproducible and collaborative biomedical analyses: 2018 update. Nucleic Acids Res. *46*, W537–W544.

59. Rhie, A., Walenz, B.P., Koren, S., and Phillippy, A.M. (2020). Merqury: Reference-free quality, completeness, and phasing assessment for genome assemblies. Genome Biol. *21*, 245.

60. Vurture, G.W., Sedlazeck, F.J., Nattestad, M., Underwood, C.J., Fang, H., Gurtowski, J., and Schatz, M.C. (2017). GenomeScope: Fast reference-free genome profiling from short reads. Bioinformatics *33*, 2202–2204.

61. Cheng, H., Concepcion, G.T., Feng, X., Zhang, H., and Li, H. (2021). Haplotype-resolved de novo assembly using phased assembly graphs with hifiasm. Nat. Methods *18*, 170–175.

62. Formenti, G., Abueg, L., Brajuka, A., Brajuka, N., Gallardo-Alba, C., Giani, A., Fedrigo, O., and Jarvis, E.D. (2022). Gfastats: Conversion, evaluation and manipulation of genome sequences using assembly graphs. Bioinformatics *38*, 4214–4216.

63. Li, H. (2018). Minimap2: Pairwise alignment for nucleotide sequences.

Bioinformatics *34*, 3094–3100.

64. Guan, D., Guan, D., McCarthy, S.A., Wood, J., Howe, K., Wang, Y., Durbin, R., and Durbin, R. (2020). Identifying and removing haplotypic duplication in primary genome assemblies. Bioinformatics *36*, 2896–2898.

65. Morgulis, A., Gertz, E.M., Schäffer, A.A., and Agarwala, R. (2006). A fast and symmetric DUST implementation to mask low-complexity DNA sequences. J. Comput. Biol. *13*, 1028–1040.

66. Wood, D.E., Lu, J., and Langmead, B. (2019). Improved metagenomic analysis with Kraken 2. Genome Biol. *20*, 257.

67. Buchfink, B., Xie, C., and Huson, D.H. (2014). Fast and sensitive protein alignment using DIAMOND. Nat. Methods *12*, 59–60.

68. Belton, J.M., McCord, R.P., Gibcus, J.H., Naumova, N., Zhan, Y., and Dekker, J. (2012). Hi-C: A comprehensive technique to capture the conformation of genomes. Methods *58*, 268–276.

69. Zhang, X., Zhang, S., Zhao, Q., Ming, R., and Tang, H. (2019). Assembly of allele-aware, chromosomal-scale autopolyploid genomes based on Hi-C data. Nat. Plants *5*, 833–845.

70. Zhan, H. (2005). Karyotype and RAPD analyses of two bethylid wasps.

71. Wan, Y., Wu, H.-J., Yang, J.-P., Zhang, J.-L., Shen, Z.-C., Xu, H.-J., and Ye, Y.-X. (2024). Chromosome-level genome assembly of the bethylid ectoparasitoid wasp *Sclerodermus* sp. '*alternatusi*.' Sci. Data *11*, 438.

72. Haas, B.J., Delcher, A.L., Mount, S.M., Wortman, J.R., Smith, R.K., Hannick, L.I., Maiti, R., Ronning, C.M., Rusch, D.B., Town, C.D., et al. (2003). Improving the Arabidopsis genome annotation using maximal transcript alignment assemblies. Nucleic Acids Res. *31*, 5654–5666.

73. Jones, P., Binns, D., Chang, H.Y., Fraser, M., Li, W., McAnulla, C., McWilliam, H., Maslen, J., Mitchell, A., Nuka, G., et al. (2014). InterProScan 5: Genome-scale protein function classification. Bioinformatics *30*, 1236–1240.

74. Cantalapiedra, C.P., Herņandez-Plaza, A., Letunic, I., Bork, P., and Huerta-Cepas, J. (2021). eggNOG-mapper v2: Functional annotation, orthology assignments, and domain prediction at the metagenomic scale. Mol. Biol. Evol. *38*, 5825–5829.

75. Käll, L., Krogh, A., and Sonnhammer, E.L.L. (2004). A combined transmembrane topology and signal peptide prediction method. J. Mol. Biol. *338*, 1027–1036.

76. Teufel, F., Almagro Armenteros, J.J., Johansen, A.R., Gíslason, M.H., Pihl, S.I., Tsirigos, K.D., Winther, O., Brunak, S., von Heijne, G., and Nielsen, H. (2022). SignalP 6.0 predicts all five types of signal peptides using protein language models. Nat. Biotechnol. *40*, 1023–1025.

77. Palmer, J.M., and Stajich, J. (2020). Funannotate v1.8.1: Eukaryotic genome

annotation. Zenodo, 10.5281/zenodo.1134477.

78. Gurevich, A., Saveliev, V., Vyahhi, N., and Tesler, G. (2013). QUAST: Quality assessment tool for genome assemblies. Bioinformatics *29*, 1072–1075.

79. Manni, M., Berkeley, M.R., Seppey, M., and Zdobnov, E.M. (2021). BUSCO: Assessing genomic data quality and beyond. Curr. Protoc. *1*, e323.

80. Allio, R., Schomaker-Bastos, A., Romiguier, J., Prosdocimi, F., Nabholz, B., and Delsuc, F. (2020). MitoFinder: Efficient automated large-scale extraction of mitogenomic data in target enrichment phylogenomics. Mol. Ecol. Resour. *20*, 892–905.

81. Donath, A., Jühling, F., Al-Arab, M., Bernhart, S.H., Reinhardt, F., Stadler, P.F., Middendorf, M., and Bernt, M. (2019). Improved annotation of protein-coding genes boundaries in metazoan mitochondrial genomes. Nucleic Acids Res. *47*, 10543–10552.

82. Dunn, N.A., Unni, D.R., Diesh, C., Munoz-Torres, M., Harris, N.L., Yao, E., Rasche, H., Holmes, I.H., Elsik, C.G., and Lewis, S.E. (2019). Apollo: Democratizing genome annotation. PLoS Comput. Biol. *15*, e1006790.

83. Mirdita, M., Steinegger, M., and Söding, J. (2019). MMseqs2 desktop and local web server app for fast, interactive sequence searches. Bioinformatics *35*, 2856–2858.

84. Van Dongen, S. (2008). Graph clustering via a discrete uncoupling process. SIAM J. Matrix Anal. Appl. *30*, 121–141.

85. Katoh, K., Misawa, K., Kuma, K.I., and Miyata, T. (2002). MAFFT: A novel method for rapid multiple sequence alignment based on fast Fourier transform. Nucleic Acids Res. *30*, 3059–3066.

86. Finn, R.D., Clements, J., and Eddy, S.R. (2011). HMMER web server: Interactive sequence similarity searching. Nucleic Acids Res. *39*, W29–W37.

87. Gotoh, O. (2024). Spaln3: improvement in speed and accuracy of genome mapping and spliced alignment of protein query sequences. Bioinformatics *40*, btae517.

88. Stanke, M., Steinkamp, R., Waack, S., and Morgenstern, B. (2004). AUGUSTUS: A web server for gene finding in eukaryotes. Nucleic Acids Res. *32*, W309–W312.

89. Emms, D.M., and Kelly, S. (2019). OrthoFinder: Phylogenetic orthology inference for comparative genomics. Genome Biol. *20*, 238.

90. Servant, N., nf-core bot, Ewels, P., Garcia, M.U., Talbot, A., Peltzer, A., Miller, E., Rossini, R., Zohren, J., Menden, K., et al. (2023). nf-core/hic: nf-core/hic v2.1.0 (2.1.0). Zenodo, 10.5281/zenodo.7994878.

91. Ramírez, F., Bhardwaj, V., Arrigoni, L., Lam, K.C., Grüning, B.A., Villaveces, J., Habermann, B., Akhtar, A., and Manke, T. (2018). High-resolution TADs reveal DNA sequences underlying genome organization in flies. Nat. Commun. *9*, 189.

92. Lieberman-Aiden, E., Van Berkum, N.L., Williams, L., Imakaev, M., Ragoczy, T., Telling, A., Amit, I., Lajoie, B.R., Sabo, P.J., Dorschner, M.O., et al. (2009). Comprehensive mapping of long-range interactions reveals folding principles of the human genome. Science *326*, 289–293.

93. Rao, S.S.P., Huntley, M.H., Durand, N.C., Stamenova, E.K., Bochkov, I.D., Robinson, J.T., Sanborn, A.L., Machol, I., Omer, A.D., Lander, E.S., et al. (2014). A 3D map of the human genome at kilobase resolution reveals principles of chromatin looping. Cell *159*, 1665–1680.

94. Hackl, T., Ankenbrand, M., Adrichem, B. van, Wilkins, D., and Haslinger, K. (2024). gggenomes: effective and versatile visualizations for comparative genomics. arXiv, 2411.13556.

95. Patel, H., Ewels, P., Peltzer, A., Botvinnik, O., Sturm, G., Moreno, D., Vemuri, P., Garcia, M.U., silviamorins, Pantano, L., et al. nf-core/rnaseq: nf-core/rnaseq v3.12.0 - Osmium Octopus (3.12.0). Zenodo, 10.5281/zenodo.7998767.

96. WackerO, Manning, J., Zoufir, A., Bot, N., Peltzer, A., Domínguez, C.T. i, Carlson, D., Möller, S., Ribeiro-Dantas, M., Patel, H., et al. (2023). nf-core/differentialabundance: v1.4.0 - 2023-11-27 (1.4.0). Zenodo, 10.5281/zenodo.7568000.

97. Love, M.I., Huber, W., and Anders, S. (2014). Moderated estimation of fold change and dispersion for RNA-seq data with DESeq2. Genome Biol. *15*, 550.

98. Concordet, J.P., and Haeussler, M. (2018). CRISPOR: Intuitive guide selection for CRISPR/Cas9 genome editing experiments and screens. Nucleic Acids Res. *46*, W242–W245.

99. Hoberecht, L., Perampalam, P., Lun, A., and Fortin, J.P. (2022). A comprehensive Bioconductor ecosystem for the design of CRISPR guide RNAs across nucleases and technologies. Nat. Commun. *13*, 6568.

100. Malabusini, S., Hardy, I.C.W., Jucker, C., Savoldelli, S., and Lupi, D. (2022). How many cooperators are too many? Foundress number, reproduction and sex ratio in a quasi-social parasitoid. Ecol. Entomol. *47*, 566–579.

101. Pan, S., Wang, C., Su, J., Huang, X., Liu, S., Hao, H., Yu, X., Li, H., Sun, J., Li, L., et al. (2025). Long-term rearing experiences influence parasitism ability of an ectoparasitoid wasp. Insect Sci.

102. Rueden, C.T., Schindelin, J., Hiner, M.C., DeZonia, B.E., Walter, A.E., Arena, E.T., and Eliceiri, K.W. (2017). ImageJ2: ImageJ for the next generation of scientific image data. BMC Bioinformatics *18*, 529.

103. Waterhouse, R.M., Seppey, M., Simao, F.A., Manni, M., Ioannidis, P., Klioutchnikov, G., Kriventseva, E. V., and Zdobnov, E.M. (2018). BUSCO applications from quality assessments to gene prediction and phylogenomics. Mol. Biol. Evol. *35*, 543–548.

104. Bonev, B., and Cavalli, G. (2016). Organization and function of the 3D genome.

Nat. Rev. Genet. *17*, 661–678.

105. Zhang, B., Yang, R.R., Jiang, X.C., Xu, X.X., Wang, B., and Wang, G.R. (2023). Genome-wide analysis of the odorant receptor gene family in *Solenopsis invicta*, *Ooceraea biroi*, and *Monomorium pharaonis* (Hymenoptera: Formicidae). Int. J. Mol. Sci. *24*, 6624.

106. Zhou, X., Slone, J.D., Rokas, A., Berger, S.L., Liebig, J., Ray, A., Reinberg, D., and Zwiebel, L.J. (2012). Phylogenetic and transcriptomic analysis of chemosensory receptors in a pair of divergent ant species reveals sex-specific signatures of odor coding. PLoS Genet. *8*, e1002930.

107. Li, L., Huang, W., Luo, L., Wei, Y., Chen, Y., and Wu, S. (2025). Underlying chemical communication in maternal care of a sub-social parasitoid *Sclerodermus guani*. Preprint at https://doi.org/10.21203/rs.3.rs-84338.

108. Fan, J., Sun, J., and Shi, J. (2007). Attraction of the Japanese pine sawyer, *Monochamus alternatus*, to volatiles from stressed host in China. Ann. For. Sci. *64*, 67–71.

109. Luo, L. (2018). Mating behavior of *Sclerodermus guani* (Hymenoptera: Bethylidae) and its mechanism of chemical ecology.

110. Haak, U., Hölldobler, B., Bestmann, H.J., and Kern, F. (1996). Species-specificity in trail pheromones and Dufour's gland contents of *Camponotus atriceps* and *C. floridanus* (Hymenoptera: Formicidae). Chemoecology *7*, 85–93.

111. Guan, D., Lu, Y.Y., Liao, X.L., Wang, L., and Chen, L. (2014). Electroantennogram and behavioral responses of the imported fire ant, solenopsis invicta Buren, to an alarm pheromone component and its analogues. J. Agric. Food Chem. *62*, 11924–11932.

112. Ferguson, S.T., Bakis, I., Edwards, N.D., and Zwiebel, L.J. (2023). Olfactory sensitivity differentiates morphologically distinct worker castes in *Camponotus floridanus*. BMC Biol. *21*, 3.

113. Wicker, T., Sabot, F., Hua-Van, A., Bennetzen, J.L., Capy, P., Chalhoub, B., Flavell, A., Leroy, P., Morgante, M., Panaud, O., et al. (2007). A unified classification system for eukaryotic transposable elements. Nat. Rev. Genet. *8*, 973–982.

114. Bourque, G., Burns, K.H., Gehring, M., Gorbunova, V., Seluanov, A., Hammell, M., Imbeault, M., Izsvák, Z., Levin, H.L., Macfarlan, T.S., et al. (2018). Ten things you should know about transposable elements. Genome Biol. *19*, 199.

115. Nanni, L., Ceri, S., and Logie, C. (2020). Spatial patterns of CTCF sites define the anatomy of TADs and their boundaries. Genome Biol. *21*, 197.

116. Ealo, T., Sanchez-Gaya, V., Respuela, P., Muñoz-San Martín, M., Martin-Batista, E., Haro, E., and Rada-Iglesias, A. (2024). Cooperative insulation of regulatory domains by CTCF-dependent physical insulation and promoter competition. Nat. Commun. *15*, 7258.

117. Davidson, I.F., Barth, R., Zaczek, M., van der Torre, J., Tang, W., Nagasaka, K., Janissen, R., Kerssemakers, J., Wutz, G., Dekker, C., et al. (2023). CTCF is a DNA-tension-dependent barrier to cohesin-mediated loop extrusion. Nature *616*, 822–827.

118. Krefting, J., Andrade-Navarro, M.A., and Ibn-Salem, J. (2018). Evolutionary stability of topologically associating domains is associated with conserved gene regulation. BMC Biol. *16*, 87.

119. McArthur, E., and Capra, J.A. (2021). Topologically associating domain boundaries that are stable across diverse cell types are evolutionarily constrained and enriched for heritability. Am. J. Hum. Genet. *108*, 269–283.

120. Liao, Y., Zhang, X., Chakraborty, M., and Emerson, J.J. (2021). Topologically associating domains and their role in the evolution of genome structure and function in *Drosophila*. Genome Res. *31*, 397–410.

121. Gong, Y., Lazaris, C., Sakellaropoulos, T., Lozano, A., Kambadur, P., Ntziachristos, P., Aifantis, I., and Tsirigos, A. (2018). Stratification of TAD boundaries reveals preferential insulation of super-enhancers by strong boundaries. Nat. Commun. *9*, 542.

122. Carlson, D.A., Mayer, M.S., Silhacek, D.L., James, J.D., Beroza, M., and Bierl, B.A. (1971). Sex attractant pheromone of the house fly: Isolation, identification and synthesis. Science *174*, 76–78.

123. Liu, W., Cai, C., Wu, J., and Wang, B. (2025). A pheromone from cuticular hydrocarbons regulates mating behavior in the hoverfly *Eupeodes corollae*. J. Integr. Agric. *24*, 4732–4743.

124. Carpita, A., Canale, A., Raffaelli, A., Saba, A., Benelli, G., and Raspi, A. (2012). (Z)-9-tricosene identified in rectal gland extracts of *Bactrocera oleae* males: First evidence of a male-produced female attractant in olive fruit fly. Naturwissenschaften *99*, 77–81.

125. Li, K.M., Ren, L.Y., Zhang, Y.J., Wu, K.M., and Guo, Y.Y. (2012). Knockdown of *Microplitis mediator* odorant receptor involved in the sensitive detection of two chemicals. J. Chem. Ecol. *38*, 287–294.

126. Drijfhout, F.P., Kather, R., and Martin, S.J. (2010). The role of cuticular hydrocarbons in insects. In Behavioral and Chemical Ecology, pp. 91–114.

127. Fan, X. Bin, Mo, B.T., Li, G.C., Huang, L.Q., Guo, H., Gong, X.L., and Wang, C.Z. (2022). Mutagenesis of the odorant receptor co-receptor (Orco) reveals severe olfactory defects in the crop pest moth *Helicoverpa armigera*. BMC Biol. *20*, 214.

128. Ma, C., Cui, S., Bai, Q., Tian, Z., Zhang, Y., Chen, G., Gao, X., Tian, Z., Chen, H., Guo, J., et al. (2020). Olfactory co-receptor is involved in host recognition and oviposition in *Ophraella communa* (Coleoptera: Chrysomelidae). Insect Mol. Biol. *29*, 381–390.

129. Li, F., Tian, J., Di, Z., Qu, C., Fu, Y., Yang, S., and Luo, C. (2024). Orco mediates

olfactory behavior and oviposition in the whitefly *Bemisia tabaci*. Pestic. Biochem. Physiol. *199*, 105773.

130. Paulo, D.F., Junqueira, A.C.M., Arp, A.P., Vieira, A.S., Ceballos, J., Skoda, S.R., Pérez-de-León, A.A., Sagel, A., McMillan, W.O., Scott, M.J., et al. (2021). Disruption of the odorant coreceptor Orco impairs foraging and host finding behaviors in the New World screwworm fly. Sci. Rep. *11*, 11379.

131. Wu, J.N., Cai, C.X., Liu, W.B., Ai, D., Cao, S., Wang, B., and Wang, G.R. (2023). Mutagenesis of odorant receptor coreceptor Orco reveals the odorant-detected behavior of the predator *Eupeodes corollae*. Int. J. Mol. Sci. *24*, 17284.

132. Sun, H., Liu, F., Ye, Z., Baker, A., and Zwiebel, L.J. (2020). Mutagenesis of the orco odorant receptor co-receptor impairs olfactory function in the malaria vector *Anopheles coluzzii*. Insect Biochem. Mol. Biol. *127*.

133. Hoffmeister, T.S. (2000). Marking decisions and host discrimination in a parasitoid attacking concealed hosts. Can. J. Zool. *78*, 1494–1499.

134. Zhang, X., and Wang, G. (2025). Sources, identification, and behavioral significance of oviposition-deterring pheromones in insects. Pest Manag. Sci. *81*, 7268–7275.

135. Stelinski, L.L., Boina, D.R., and Meyer, W.L. (2010). Oviposition marking behavior of *Diachasma alloeum*, (Hymenoptera: Braconidae), parasitizing *Rhagoletis pomonella*, (Diptera: Tephritidae). J. Insect Behav. *23*, 419–430.

136. Wang, Z.Y., Yin, S.Y., Wei, J.R., Qiu, L.F., Hu, H.Y., and Liu, P.C. (2025). Marking and deterring oviposition on parasitized hosts by a host-marking pheromone in an egg parasitoid. J. Chem. Ecol. *51*, 66.

137. Rosi, M.C., Isidoro, N., Colazza, S., and Bin, F. (2001). Source of the host marking pheromone in the egg parasitoid *Trissolcus basalis* (Hymenoptera: Scelionidae). J. Insect Physiol. *47*, 989–995.

138. Li, G., Chen, Y., Wu, S., Li, L., Wei, Y., and Zhang, M. (2025). Dynamics of ovarian development during parental caring in adult females of ectoparasitoid *Sclerodermus guani* (Hymenoptera: Bethylidae). Acta Entomol. Sin. *68*, 983–998.

139. Szabo, Q., Bantignies, F., and Cavalli, G. (2019). Principles of genome folding into topologically associating domains. Sci. Adv. *5*, eaaw1668.

140. Dixon, J.R., Gorkin, D.U., and Ren, B. (2016). Chromatin domains: The unit of chromosome organization. Mol. Cell *62*, 668–680.

## Acknowledgements

We thank all members of the FL lab for suggestions and comments. We thank Guizhou Normal University, Shenzhen Bay Laboratory, and Novogene for equipment and

technical support. We are also very grateful to Li Li's lab at Guizhou Normal University for their guidance and support in insect rearing.

**Funding:**

National Natural Science Foundation of China, Grant No. 32401587 (ZY)

Guizhou Provincial Science and Technology Department, Grant No. Qian Ke He Ji Chu ZK [2024] General 423 (ZY)

Guizhou Normal University, Grant No. QSXM [2022] B09 (ZY)

National Natural Science Foundation of China, Grant No. 82372289 and 82561128263 (FL)

Guangdong Pearl River Funding, Grant No. 2023QN10Y093 (FL)

National Natural Science Foundation of China, Grant No. 82350410493 (STF)

Shenzhen Medical Special Fund, Grant No. A032400171 (STF)

**Author contributions:**

ZY, STF, GF, and FL designed research; ZY, STF, GF, JFO, ZY, TG, and XZ performed research; ZY, STF, GF, JFO, TG, and XZ analyzed data; ZY, STF, GF, JFO, and FL wrote the paper. All authors approved the manuscript.

**Competing interests:**

Authors declare that they have no competing interests.

**Data and materials availability:** All data generated or analyzed are included in this published article and its supplementary information files. The *Sclerodermus guani* genome assembly was submitted to NCBI under BioProject number PRJNA1147886, BioSample SAMN56416872. The transcriptomic data was submitted to the same BioProject (PRJNA1147886), BioSamples SAMN43173872- SAMN43173881.

## Figures

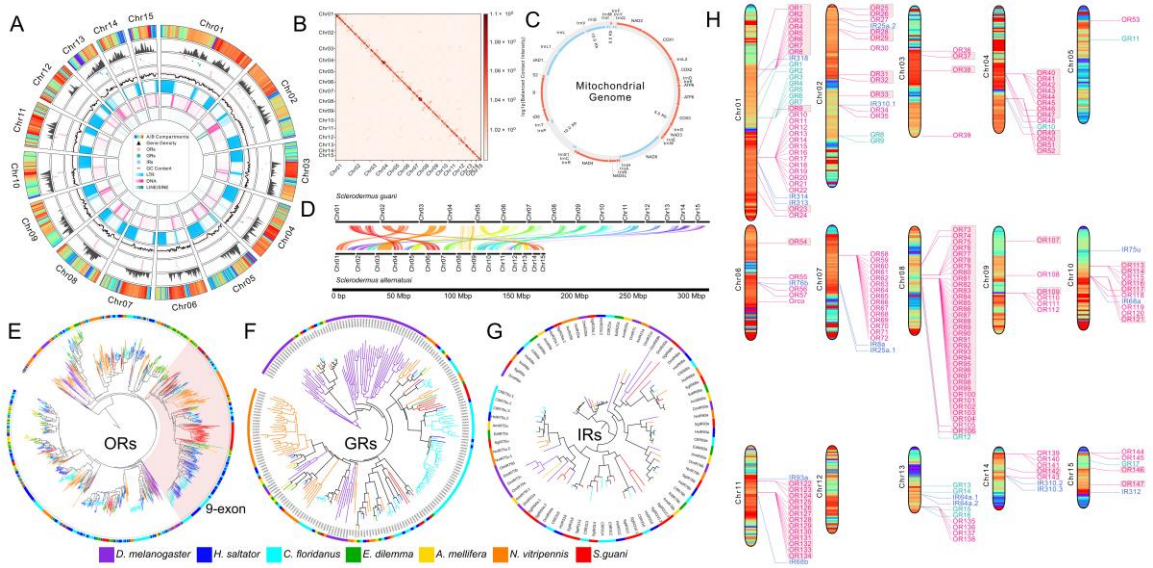


**Fig. 1.** Chromosome-level assembly and genome architecture of *S. guani*. **(A)** Nuclear genome circos plot summarizing chromosomal organization and genomic features. From outer to inner rings: chromosome ideograms colored by A/B compartment principal component (PC1) scores (warm colors, A compartment; cool colors, B compartment); gene density (filled line graph); chemoreceptor gene locations (odorant receptors, pink; gustatory receptors, green; ionotropic receptors, blue); GC content (line graph; dashed red line indicates 50% GC); long terminal repeat (LTR) density; DNA repeat density; and LINE/SINE density. All genomic features were calculated in 250-kb bins. **(B)** Whole-genome Hi-C contact map at 640-kb resolution, demonstrating chromosome-scale scaffolding. **(C)** Circular mitochondrial genome showing gene content and orientation. Protein-coding genes, tRNAs, and rRNAs are shown with strand orientation indicated (salmon, forward; cyan, reverse). **(D)** Synteny ribbon plot between *S. guani* and *S. alternatusi*, each comprising 15 chromosomes. **(E-G)** Maximum-likelihood phylogeny of odorant receptors (ORs), gustatory receptors (GRs), and ionotropic receptors (IRs) from *S. guani* (red), *Nasonia vitripennis* (orange), *Apis mellifera* (yellow), *Euglossa dilemma* (green), *Camponotus floridanus* (cyan), *Harpegnathos saltator* (blue), and *Drosophila melanogaster* (violet). The shaded red clade highlights the Hymenopteran-specific 9-exon family. **(H)** Karyotype-style representation of the 15 chromosome-level scaffolds of *S. guani*. Chromosomes are colored by A/B compartment principal component (PC1) scores (warm colors, A compartment; cool colors, B compartment). Chemosensory receptor loci are shown as leader lines extending from their genomic position to gene labels (odorant receptors, pink; gustatory receptors, green; ionotropic receptors, blue). The shaded red boxes highlight members of the Hymenopteran-specific 9-exon family.

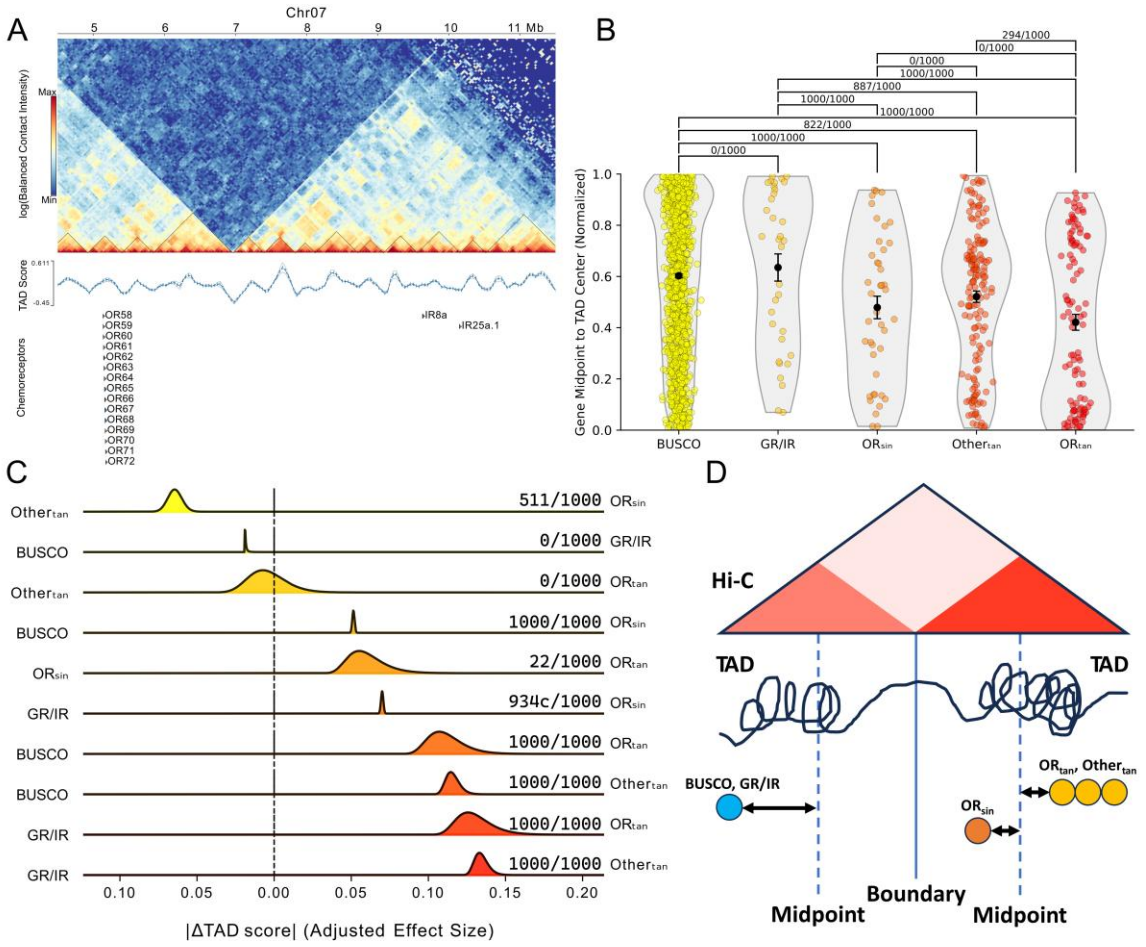


**Fig. 2.** Odorant receptors occupy distinct 3D chromatin environments. **(A)** Hi-C contact map of chromosome 7 at 40-kb resolution with topologically associating domains (TADs) outlined in black. Below the contact map, the insulation (TAD) score is plotted as a line graph. Chemosensory gene locations are shown beneath, highlighting a large tandem array of ORs associated with elevated TAD scores. **(B)** Normalized distance from gene midpoint to TAD center across gene classes: BUSCO single-copy orthologs (BUSCO), gustatory and ionotropic receptors (GR/IR), odorant receptor singletons (ORsin), non-OR tandem array genes (Othertan), and odorant receptors in tandem arrays (ORtan). Black point and lines represent mean±SEM. Significance stability is indicated by the number of significant bootstrap iterations. **(C)** Distribution of adjusted effect sizes (ΔTAD score) from pairwise mixed-model comparisons across 1,000 bootstrap iterations. Significance stability is indicated by the number of significant bootstrap iterations. **(D)** Conceptual model illustrating differential positioning of gene classes within TADs. Both OR singletons and ORs and other gene families in tandem array preferentially localize toward TAD centers relative to BUSCO, GR, and IR singleton genes.

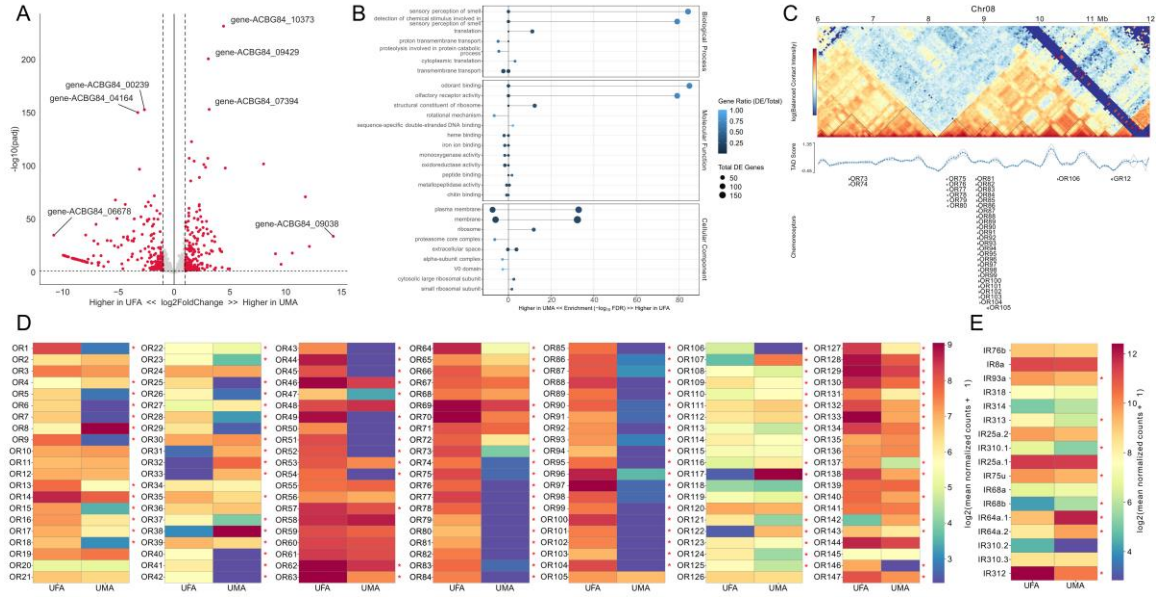


**Fig. 3.** Sex-biased transcription of chemoreceptors and chromatin context. **(A)** Volcano plot showing differential gene expression between UFA and UMA antennae. The short-dashed horizontal line indicates adjust P = 0.05. Red points represent significantly differentially abundant transcripts (202 up in UFA, 209 up in UMA), and gray points represent non-significant transcripts. **(B)** GO enrichment mirror plot for differentially expressed genes in UFA versus UMA. **(C)** Hi-C contact map of chromosome 8 (40-kb bins) with TADs outlined in black and insulation score plotted below. Two large tandem OR arrays (OR75–80 and OR81–104) are highlighted and correspond to receptors significantly upregulated in UFA. **(D)** Heatmap of log2(mean normalized counts + 1) for all 147 tuning ORs in UFA and UMA. Significantly differentially abundant receptors (padj < 0.05) are marked with red asterisks. **(E)** Heatmap of log2(mean normalized counts + 1) for all 17 ionotropic receptors. Significantly differentially abundant receptors (padj < 0.05) are marked with red asterisks.

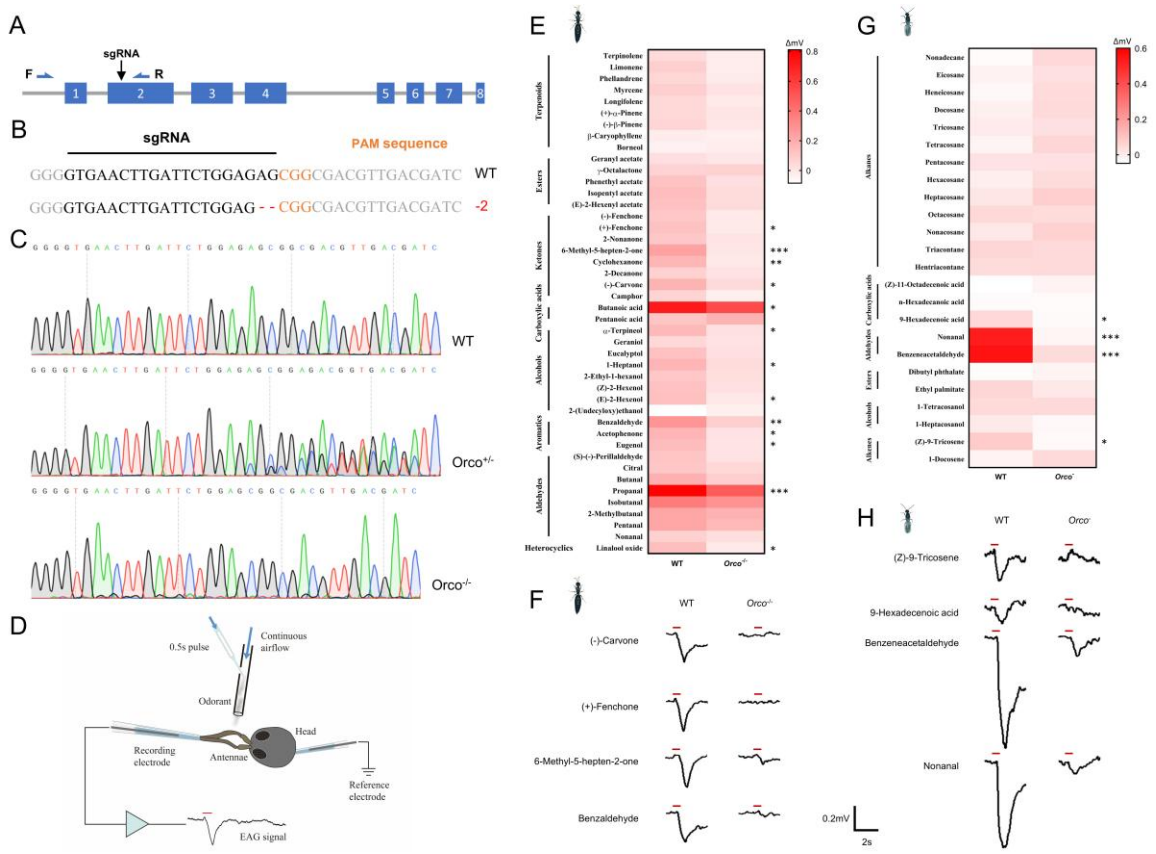


**Fig. 4.** Mutagenesis and electrophysiological responses of *S. guani*. **(A)** Schematic of the *Orco* gene structure and PCR verification strategy. Exons 1-8 are shown as solid boxes. The sgRNA target site (black arrow) indicates Cas9-mediated double-strand break site within exon 2. Primers (F/ R) flanking the target site were used to generate an amplicon for sequencing. **(B)** Target site sequence in wild-type (WT) and *Orco* mutant alleles. The sgRNA sequence is shown in black, and the protospacer adjacent motif (PAM) is highlighted in orange. The -2bp deletion mutation is indicated by red dashes. **(C)** Sanger sequencing chromatograms of the target site from a wild-type (WT), heterozygous ($Orco^{+/-}$), and homozygous mutant ($Orco^{-/-}$) female individual. The heterozygous sample shows overlapping peaks downstream of the cleavage site, confirming a bi-allelic genotype. **(D)** Schematic diagram of EAG experiment on *S. guani*. **(E)** Female EAG responses. Heatmap shows mean response amplitudes (ΔmV) for wild-type (WT) and $Orco^{-/-}$ females to a panel of odorants. The response scale ranges from -0.085 to 0.810 mV. Asterisks denote significant differences between genotypes for each odorant determined by multiple t-tests: P value < 0.05 (*); P value < 0.01 (**); P value < 0.001 (***). **(F)** Representative EAG recordings of wild-type (WT) and $Orco^{-/-}$ females in response to a panel of stimuli. **(G)** Male EAG responses. Heatmap shows mean response amplitudes (ΔmV) for wild-type (WT) and $Orco^{-}$ males. The response scale ranges from -0.048 to 0.600 mV. Statistical comparisons between genotypes for each odorant are indicated as in (**E**). **(H)** Representative EAG recordings of wild-type (WT)

1585 and *Orco*$^{-}$ males in response to a panel of stimuli. The red bars indicate stimulus duration
1586 (0.5s).

1587

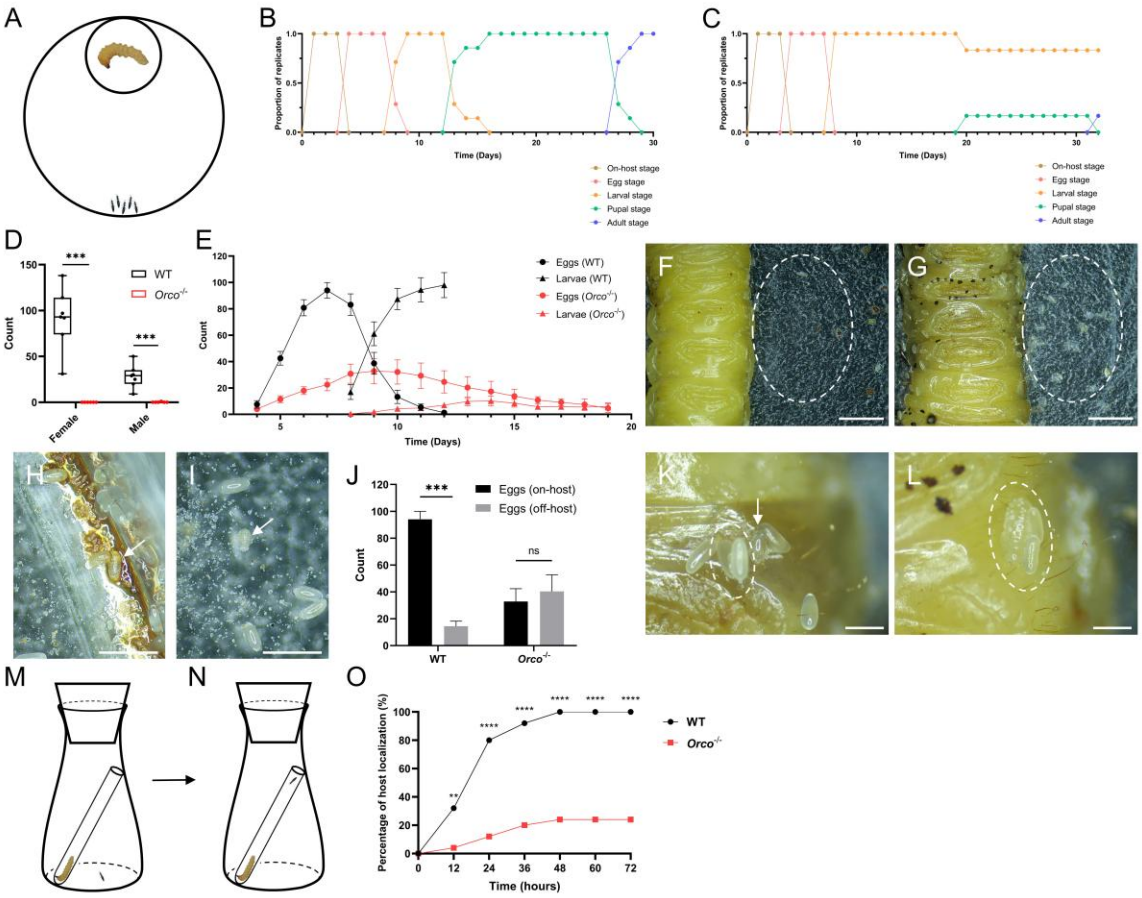


**Fig. 5.** Reproductive and host-seeking assays. **(A)** Schematic of the parasitizing assay. A *M. alternatus* larva was confined in a small Petri dish and five anesthetized *S. guani* females were released in the large Petri dish to perform parasitism. **(B, C)** Cumulative percentage of broods established by wild-type (**B**) and *Orco*$^{-/-}$ (**C**) females reaching successive developmental stages (egg, larva, pupa, adult) over time. **(D)** Box plot of adult offspring number in broods established by wild-type (WT) and *Orco*$^{-/-}$ females. Multiple t-tests using Holm-Sidak method (n = 6-7) suggest both female and male offspring of wild-type females is significantly more than those of *Orco*$^{-/-}$ females. **(E)** Daily egg and larval count produced by wild-type and *Orco*$^{-/-}$ females. Multiple t-tests using Holm-Sidak method (n = 6-7) suggest wild-type females laid significantly more eggs than *Orco*$^{-/-}$ females from Day 5 to Day 8 (Adjusted P value < 0.01). **(F, G)** Representative images of egg distribution in wild-type (**F**) and *Orco*$^{-/-}$ (**G**) broods. The off-host eggs are circled with dashed lines. Scale bar = 5 mm. **(H)** Representative image of eggs deposited by *Orco*$^{-/-}$ females in excretion (highlighted by an arrow). Scale bar = 1 mm. **(I)** Representative image of an off-host larva (highlighted by an arrow). Scale bar = 1 mm. **(J)** Number of eggs laid on-host and off-host by wild-type and *Orco*$^{-/-}$ females at the time points with maximum egg count (Day 7 for the wild-type brood vs. Day 9 for the *Orco*$^{-/-}$ brood). Multiple t-tests using Holm-Sidak method (n = 6-7) suggest wild-type females

oviposit significantly more eggs on host, while *Orco*$^{-/-}$ females oviposit indiscriminately. **(K)** Aberrant egg-laying by *Orco*$^{-/-}$ females: eggs stacked on existing eggs (dashed lines) and subsequent larval cannibalism (arrow). Scale bar = 0.5 mm. **(L)** Representative image of eggs laid on an existing larva (highlighted by dashed lines). Scale bar = 0.5 mm. **(M)** Schematic of the host-seeking assay. A *M. alternatus* larva was confined in a glass test tube within a conical flask. A female *S. guani* female was introduced to the bottom of the flask and allowed to locate the host over 72hrs. **(N)** Successful host localization was defined as the wasp's entry into the host-containing tube. **(O)** Percentage of host localization using wild-type and *Orco*$^{-/-}$ female wasps. Chi-square tests suggest significant difference at all time points. Significance levels are depicted with asterisks: P value < 0.01 (**); P value < 0.001 (***); P value < 0.0001 (****). Error bars = SEM. ns, not significant.

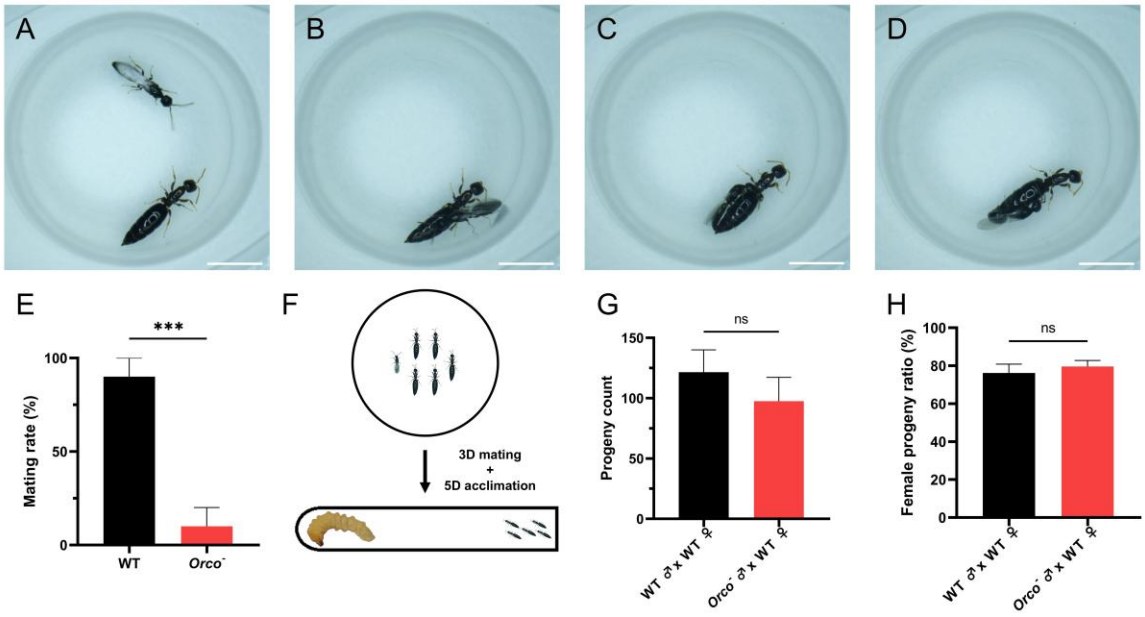


**Fig. 6.** Mating assays. **(A)** Schematic of the mating assay. A single virgin male was paired with a virgin wild-type female in a confined chamber for 10 minutes. Scale bar = 2 mm. **(B-D)** Sequential images depicting characteristic wild-type (WT) male copulation behaviors: antennal tapping (**B**), mounting (**C**), and genitalia insertion (**D**). Scale bar = 2 mm. **(E)** Mating success rate of WT and *Orco*$^{-}$ males in the assay. T-test suggests WT males manifest significantly higher mating efficiency than *Orco*$^{-}$ males (n = 10). **(F)** Schematic of the long-term mating assay. A single virgin male was housed with five virgin WT females for 72 hours. The females were then provided a host larva for parasitism. **(G)** Total progeny number from the long-term mating assay. No significant difference was found between males of the two genotypes (t-tests; n = 4-6). **(H)** Female progeny ratio from the long-term mating assay. No significant difference was found between males of the two genotypes (t-tests; n = 4-6). Significance levels are depicted with asterisks: P value < 0.001 (***). Error bars = SEM. ns, not significant.

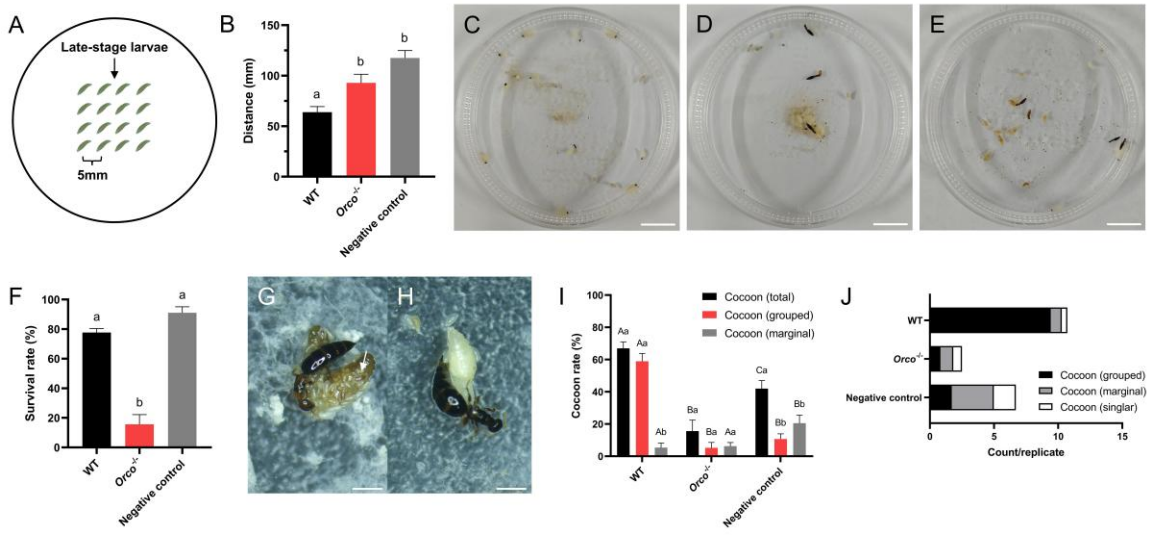


**Fig. 7.** Maternal care assays. **(A)** Schematic of the larval-translocation assay. Sixteen late-instar larvae were arranged in the center equidistantly (~5mm). **(B)** Nearest-neighbor distance among larvae after 72 hours, indicative of clustering behavior. One-way ANOVA suggests wild-type females performed significantly better in larval clustering. Different lowercase letters denote statistically significant differences (n = 6-7; P value < 0.05). **(C-E)** Representative images of larval distribution and cocoon formation after 72hrs in the presence of no female (**C**, negative control), wild-type females (**D**), or *Orco*$^{-/-}$ females (**E**) females. Scale bar = 10 mm. **(F)** Adult survival rate after emergence. One-way ANOVA suggests the presence of *Orco*$^{-/-}$ females significantly reduced offspring survival. Different lowercase letters denote statistically significant differences (n = 6-7; P value < 0.05). **(G, H)** Aberrant intraspecific oviposition by *Orco*$^{-/-}$ females on larvae (**G**) and pupae (**H**), leading to offspring cannibalism (**G**; arrow). Scale bar = 1 mm. **(I)** Proportion of larvae that successfully formed cocoons, categorized by placement (grouped and marginal). Two One-way ANOVA analyses were performed and distinguished with upper- and lowercase letters. Uppercase letters compare the same cocoon type across different female treatments (WT vs. *Orco*$^{-/-}$ vs. negative control); lowercase letters compare all cocoon types within the same treatment. Different letters indicate significant differences (n = 6-7; P value < 0.05). **(J)** Distribution of cocoons across the three possible configurations for each experimental group. Error bars = SEM.

## Supplementary Materials

**Fig. S1.** GenomeScope k-mer profiling. GenomeScope analysis of sequencing reads.

**Fig. S2.** Genome completeness assessment. **(A)** Genome-level Arthropoda BUSCO results (98.4% complete; 96.2% single copy, 2.2% duplicated, 0.9% fragmented, 0.7% missing). **(B)** Protein-level BUSCO results (92.3% complete; 90.2% single copy, 2.0% duplicated, 4.1% fragmented, 3.7% missing).

**Fig. S3.** Chromosome length distribution. Bar graph showing lengths of 15 assembled chromosomes, 50 unplaced contigs, and the mitochondrial genome.

**Fig. S4.** Chromosome-scale Hi-C maps. Hi-C contact maps for all 15 chromosomes at 40-kb resolution.

**Fig. S5.** Comparative chemoreceptor repertoire sizes. Stacked bar graph showing total OR (pink), GR (green), and IR (blue) counts in *S. guani*, *N. vitripennis*, *A. mellifera*, *E. dilemma*, *C. floridanus*, *H. saltator*, and *D. melanogaster*.

**Fig. S6.** Adult mass measurement. T-tests suggest no significant differences in adult weights between wild-type and *Orco* mutant females **(A)** (n = 27-28) and males **(B)** (n = 7). ns, not significant. Error bars = SEM.

**Fig. S7.** Egg eclosion rate. T-test suggests no significant differences in eclosion rate between wild-type and *Orco* mutant eggs (n = 7). ns, not significant. Error bars = SEM.

**Table S1.** Assembly statistics.

**Table S2.** Repetitive content.

**Table S3.** TAD Mixed linear model results (N = 1000).

**Table S4.** Odorant lists used in female *S. guani* electroantennogram.

**Table S5.** Odorant lists used in male *S. guani* electroantennogram.

**References.**